Cellular/Molecular

Regulation of Hippocampal Memory by mTORC1 in Somatostatin Interneurons

Julien Artinian, Alexander Jordan, Abdessattar Khlaifia, Eve Honoré, Alexandre La Fontaine, Anne-Sophie Racine, Isabel Laplante, and Jean-Claude Lacaille

Department of Neuroscience and Groupe de Recherche sur le Système Nerveux Central (CNS Research Group), Université de Montréal, Montreal QC H3C 3J7, Canada

Translational control of long-term synaptic plasticity via Mechanistic Target Of Rapamycin Complex 1 (mTORC1) is crucial for hippocampal learning and memory. The role of mTORC1 is well characterized in excitatory principal cells but remains largely unaddressed in inhibitory interneurons. Here, we used cell-type-specific conditional knock-out strategies to alter mTORC1 function selectively in somatostatin (SOM) inhibitory interneurons (SOM-INs). We found that, in male mice, upregulation and downregulation of SOM-IN mTORC1 activity bidirectionally regulates contextual fear and spatial memory consolidation. Moreover, contextual fear learning induced a metabotropic glutamate receptor type 1 (mGluR1)-mediated late long-term potentiation (LTP) of excitatory input synapses onto hippocampal SOM-INs that was dependent on mTORC1. Finally, the induction protocol for mTORC1-mediated late-LTP in SOM-INs regulated Schaffer collateral pathway LTP in pyramidal neurons. Therefore, mTORC1 activity in somatostatin interneurons contributes to learning-induced persistent plasticity of their excitatory synaptic inputs and hippocampal memory consolidation, uncovering a role of mTORC1 in inhibitory circuits for memory.

Key words: hippocampus; memory consolidation; metaplasticity; mTORC1; somatostatin interneurons; synaptic plasticity

Significance Statement

Memory consolidation necessitates synthesis of new proteins. Mechanistic Target Of Rapamycin Complex 1 (mTORC1) signaling is crucial for translational control involved in long-term memory and in late long-term potentiation (LTP). This is well described in principal glutamatergic pyramidal cells but poorly understood in GABAergic inhibitory interneurons. Here, we show that mTORC1 activity in somatostatin interneurons, a major subclass of GABAergic cells, is important to modulate long-term memory strength and precision. Furthermore, mTORC1 was necessary for learning-induced persistent LTP at excitatory inputs of somatostatin interneurons that depends on type I metabotropic glutamatergic receptors in the hippocampus. This effect was consistent with a newly described role of these interneurons in the modulation of LTP at Schaffer collateral synapses onto pyramidal cells.

Introduction

Long-term synaptic plasticity is a prime candidate cellular substrate for learning and memory (Whitlock et al., 2006; Kandel et al., 2014; Choi et al., 2018). In the hippocampus, long-term potentiation (LTP) at excitatory synapses of pyramidal cells is crucial for contextual as well as spatial learning and memory (Nicoll, 2017). In analogy to long-term memory consolidation, LTP in pyramidal cells displays an early phase, lasting minutes that is mediated by posttranslational changes, and a late phase, lasting hours that requires transcription and translation (Abel et al., 1997; Kandel et al., 2014). Mechanistic Target of Rapamycin (mTOR) is a serine/threonine kinase that associates with two distinct protein complexes, mTOR Complex 1 and 2 (mTORC1 and 2), to control cell growth, proliferation and migration (Saxton and Sabatini, 2017). mTORC1, of which Raptor is an essential component, plays a central role in cell growth by regulating protein synthesis and turnover, as well as lipid, nucleotide and

Received March 27, 2019; revised July 24, 2019; accepted Aug. 31, 2019.

Author contributions: J.A., I.L., and J.-C.L. designed research; J.A., A.J., A.K., E.H., A.L.F., A.-S.R., and I.L. performed research; J.A., A.J., A.K., E.H., A.L.F., A.-S.R., and I.L. analyzed data; J.A. wrote the first draft of the paper; J.A., I.L., and J.-C.L. edited the paper; J.A., I.L., and J.-C.L. wrote the paper.

This work was supported by the Canadian Institutes of Health Research (Grant PJT-153311to J.-C.L.) and the Fonds de la Recherche du Québec en Santé (FRQS Group Grant to J.-C.L.; Groupe de Recherche sur le Système Nerveux Central (GRSNC). J.-C.L. is the recipient of the Canada Research Chair in Cellular and Molecular Neurophysiology (950-231066). J.A. was supported by GRSNC and FRQS fellowships. A.L.F. was supported by a FRQS Fellowship. We thank J. Pepin for help with slice cultures and chemical late-LTP experiments, and members of the Lacaille laboratory for helpful discussions and comments on the manuscript. Requests for materials should be addressed to J.-C.L.

The authors declare no competing financial interests.

J. Artinian's present address: Laboratory of Nutrition and Integrated Neurobiology (NutriNeuro), INRA UMR 1286, Université de Bordeaux, 146 rue Léo Saignat, 33076 Bordeaux cedex, France.

Correspondence should be addressed to Jean-Claude Lacaille at jean-claude.lacaille@umontreal.ca.

https://doi.org/10.1523/JNEUROSCI.0728-19.2019

glucose metabolism (Saxton and Sabatini, 2017). In mature neurons, mTORC1 regulates protein synthesis during long-lasting synaptic plasticity and memory (Costa-Mattioli et al., 2009; Ran et al., 2009). This role of mTORC1 in hippocampal memory was clearly established in principal cells (Costa-Mattioli et al., 2009).

In the hippocampus, excitatory neurons are regulated by highly heterogeneous inhibitory interneurons that display various morphological and physiological properties, as well as diverse patterns of connectivity and protein expression (Pelkey et al., 2017). Plasticity of hippocampal interneurons is also implicated in learning. Hippocampus-dependent learning is associated with structural plasticity of interneuron afferent connectivity (Ruediger et al., 2011) and modulation of their excitatory inputs (Polepalli et al., 2017). In addition, excitatory synapses onto hippocampal interneurons demonstrate multiple forms of LTP (Pelletier and Lacaille, 2008; Kullmann et al., 2012). However, whether mTORC1 plays a role in these learning-related changes in inhibitory interneurons remains mostly unknown.

In the hippocampus, somatostatin (SOM) expressing interneurons (SOM-INs) are a subgroup of GABAergic interneurons that, in CA1, receive excitation from local principal pyramidal cells and provide feedback dendritic inhibition (Pelkey et al., 2017). They include the so-called Oriens-Lacunosum/Moleculare (O-LM) cells, bistratified cells and long-range projecting cells (Pelkey et al., 2017). SOM-INs regulate pyramidal cell synaptic integration (Lovett-Barron et al., 2012), control their rate and burst firing (Royer et al., 2012), modulate their synaptic plasticity (Leão et al., 2012) and support contextual fear learning (Lovett-Barron et al., 2014).

Excitatory synapses onto SOM-INs express a form of LTP dependent on type 1a metabotropic glutamate receptors (mGluR1a) (Perez et al., 2001; Vasuta et al., 2015). Additionally, a late form of mGluR1a-dependent LTP is present in O-LM interneurons in slice cultures (Ran et al., 2009) that lasts 24 h and is dependent on mTORC1-mediated translation (Ran et al., 2009, 2012). Therefore, SOM-INs represent an interesting subpopulation of interneurons to investigate mTORC1 function.

To determine whether mTORC1 activity in SOM-IN plays a role in hippocampal memory, we used conditional knock-out mouse strategies to bidirectionally manipulate mTORC1 activity selectively in SOM-INs by targeting an essential component of mTORC1, the Regulatory-Associated Protein of mTOR (Raptor), or a repressor of mTORC1, the Tuberous Sclerosis Complex 1 (TSC1). We found that mTORC1 activity in somatostatin interneurons contributes to hippocampus-dependent memory formation and to learning-induced persistent plasticity at somatostatin interneuron input synapses, uncovering an important function of mTORC1 activity in inhibitory local circuits for memory consolidation.

Materials and Methods

Subjects. All animal procedures and experiments were performed in accordance with the Université de Montréal animal care committee regulations. Mice were group housed (2–4 per cage), maintained with food and water *ad libitum* and on a 12 h light/dark cycle with all testing performed during the light phase. Knock-in mice with an internal ribosome entry site (IRES)-linked Cre recombinase gene downstream of the *Sst* locus (*Sst*$^{ires\text{-}Cre}$ mice, The Jackson Laboratory, RRID:IMSR_JAX:013044). *Sst*$^{ires\text{-}Cre}$ mice were crossed with *Rosa26*$^{lsl\text{-}EYFP}$ reporter mice (Ai3, RRID:IMSR_JAX:007903) for Cre-dependent enhanced yellow fluorescent protein (EYFP) expression in SOM-INs. *Sst*$^{ires\text{-}Cre}$;*Rosa26*$^{lsl\text{-}EYFP}$ mice were crossed with floxed *Rptor* mice (RRID:IMSR_JAX:013188) for cell-specific knock-out of *Rptor* in SOM cells. *Sst*$^{ires\text{-}Cre}$;*Rosa26*$^{lsl\text{-}EYFP}$;*Rptor*$^{WT/fl}$ heterozygous offsprings were backcrossed together to obtain *Sst*$^{ires\text{-}Cre}$;*Rosa26*$^{lsl\text{-}EYFP}$;*Rptor*$^{fl/fl}$ homozygous knock-out mice (termed Som-Raptor-KO mice), and compared with the *Rptor* wild-type mice *Sst*$^{ires\text{-}Cre}$;*Rosa26*$^{lsl\text{-}EYFP}$;*Rptor*$^{WT/WT}$ (termed Som-Raptor-WT mice). All strains were maintained on a C57BL/6N background. *Sst*$^{ires\text{-}Cre}$;*Rosa26*$^{lsl\text{-}EYFP}$ mice were crossed with floxed *Tsc1* mice (RRID:IMSR_JAX:005680) for cell-specific knock-down of *Tsc1* in SOM cells. *Sst*$^{ires\text{-}Cre}$;*Rosa26*$^{lsl\text{-}EYFP}$;*Tsc1*$^{WT/fl}$ heterozygous offsprings (termed Som-TSC1-KO mice) were compared with *Sst*$^{ires\text{-}Cre}$;*Rosa26*$^{lsl\text{-}EYFP}$;*Tsc1*$^{WT/WT}$ control mice (termed Som-TSC1-WT mice).

Molecular biology and immunohistochemistry experiments were performed on mice of both sex, electrophysiology experiments in mature acute slices and behavioral tests were performed on male mice only.

EYFP-labeled interneuron distribution. Distribution of EYFP-labeled interneurons was determined by fluorescence microscopy from hippocampal sections of Som-Raptor-WT and Som-Raptor-KO mice (6–12 weeks old). Animals were deeply anesthetized intraperitoneally with sodium pentobarbital (MTC Pharmaceuticals), perfused transcardially with ice-cold 0.1 M phosphate buffer (PB) and 4% para-formaldehyde in 0.1 M PB (PFA) and the brain isolated. Postfixed brains were cryoprotected in 30% sucrose and coronal brain sections (50 μm thick) were obtained using freezing microtome (SM200R; Leica). Sections were mounted in ProLong Gold (Invitrogen) and examined using an epifluorescence microscope (Eclipse E600; Nikon). EYFP-positive interneuron density was assessed in the hippocampal CA1 oriens layer.

Hippocampal slice culture. Organotypic hippocampal slice cultures were obtained from Som-Raptor-WT and Som-Raptor-KO mice (4–5 d-old), as described previously (Ran et al., 2009). In brief, the brain was removed and dissected in HBSS (Invitrogen)-based medium. Corticohippocampal slices (400 μm thick) were then obtained using a McIlwain tissue chopper (Cavey Laboratory Engineering). After dissection, slices were placed on Millicell culture plate inserts (Millipore) in OptiMEM (Invitrogen) supplemented with Glutamax I and horse serum (Invitrogen) kept at 37°C in a humidified atmosphere (95% air, 5% CO_2) for 3–7 d.

Chemical induction protocol for late-LTP. Slices received three applications (10 min duration each at 30 min intervals) of the mGluR1/5 agonist (S)-3,5-dihydroxyphenylglycine (DHPG, 5 μM; Abcam) in the presence of the mGluR5 antagonist 2-methyl-6 (phenylethynyl)-pyridine (MPEP, 25 μM; Tocris Bioscience). Inhibitors were applied concomitantly from 30 min before to 30 min after DHPG/MPEP treatment. LY367385, rapamycin and PP242 were from Tocris Bioscience, Millipore, and LC Laboratories, respectively. After treatments, cultured and acute slices were allowed to recover for 24 and 2 h, respectively, before recordings. Experimenters were blinded to all treatment groups and mice genotype.

Immunofluorescence. Colocalization of Raptor immunofluorescence was determined in EYFP-positive interneurons. Coronal brain sections (50 μm thick) were permeabilized with 0.5% Triton X-100 in PBS (15 min) and unspecific binding was blocked with 10% normal goat serum in 0.1% Triton X-100/PBS (1 h). Mouse monoclonal Raptor (1/500; Millipore catalog #05–1470, RRID:AB_11212192) antibody was incubated 48 h at 4°C. Sections were subsequently incubated at room temperature with Rhodamine-conjugated goat anti-mouse IgG1 (1/200; 90 min; Jackson Immunoresearch Laboratories). Sections were mounted in ProLong Gold and imaged as for EYFP-labeled interneuron distribution. The number of EYFP-positive interneurons in CA1 stratum oriens with colocalization of Raptor immunofluorescence were counted and expressed as percentage of the total EYFP-positive cells.

Colocalization of somatostatin immunofluorescence in EYFP-labeled interneurons was performed on organotypic slices obtained as described before. Slices were fixed during 24 h with 4% PFA, cryoprotected in 30% sucrose and resectioned (50 μm thick) using freezing microtome. Sections were permeabilized 30 min with 0.5% Triton X-100/PBS and unspecific binding blocked as above. Sections were incubated overnight at 4°C with rabbit polyclonal somatostatin 28 antibody (1/2000; Abcam catalog #ab43862, RRID:AB_882645) and subsequently at room temperature with Alexa Fluor 594-conjugated goat anti-rabbit IgGs (1/500, 90 min; Abcam). Sections were mounted, imaged and colocalization measured as described above for Raptor immunofluorescence.

S6 immunophosphorylation assay. Mice (3–5 weeks old) were deeply anesthetized with sodium pentobarbital and perfused transcardially with ice-cold ACSF containing the following (in mM): 110 choline-chloride, 2.5 KCl, 7 MgCl2, 26 NaHCO3, 7 dextrose, 1.3 ascorbic acid and 0.5 CaCl2, and saturated with 95% O_2-5% CO_2. Coronal hippocampal slices (300 μm) were obtained using a vibratome (VT 1000S; Leica) and transferred at room temperature into normal oxygenated ACSF containing the following (in mM): 124 NaCl, 2.5 KCl, 1.25 NaH_2PO_4, 2 $MgCl_2$, 2 $CaCl_2$, 26 $NaHCO_3$, 10 dextrose, 1.3 ascorbic acid. After a 1 h recovery period, slices received the late-LTP chemical induction protocol at 31–33°C as described above. Slices were fixed after treatment and cryoprotected in 30% sucrose 24 h later. Slices were resectioned in 50 μm thick sections using a freezing microtome (SM200R; Leica). Sections were permeabilized with 0.3% Triton X-100 in PBS (15 min) and unspecific binding was blocked with 10% normal goat serum in 0.1% Triton X-100/PBS (1 h). Rabbit polyclonal phospho-S6 ribosomal protein (1/200; anti-phospho-S6S235/236; Cell Signaling Technology catalog #2211 also 2211L, 2211S, RRID:AB_331679) antibodies were incubated 48 h at 4°C. Sections were subsequently incubated at room temperature with Alexa Fluor 594-conjugated goat anti-rabbit IgGs (1/500; 90 min; Jackson Immunoresearch). Images were acquired using a confocal microscope (LSM510; Zeiss) at excitation 488 and 543 nm. Images from different treatment/groups were acquired using the exact same parameters. Cell fluorescence was quantified using Fiji (ImageJ) by comparing integrated density in cells corrected for background.

Western blotting. Total hippocampus (10 weeks-old mice) and slice cultures (3 slices cortex-free pooled per sample) were collected and protein extracted using ice-cold radioimmunoprecipitation assay buffer containing the following: 50 mM Tris pH 7.4, 150 mM NaCl, 2 mM EDTA, 1% Triton X-100, 0.5% sodium desoxycholate, 0.1% SDS (SDS), 200 μM NaF, 200 μM Na_3VO_4 and protease inhibitor (Cocktail inhibitor set I; Millipore) (20 min, 4°C). Lysates were centrifuged at 19,000 × *g* (20 min, 4°C) and protein concentration from supernatant was determined according to bicinchoninic acid method using bovine serum albumin as standard. Fifteen to 30 μg of proteins (slice culture or total hippocampus extracts respectively) were separated by 7% (Raptor) or 12% (p-S6) SDS-PAGE and transferred onto polyvinilidene fluoride membrane. The membranes were blocked with 5% nonfat skin milk dissolved in Tris-buffered saline-0.1% Tween 20 pH 7.4 (1h30, room temperature) and incubated with rabbit polyclonal anti-phospho-$S6^{S235/236}$ (1/1000; Cell Signaling Technology, RRID:AB_331679) or rabbit monoclonal anti-Raptor (1/500; Cell Signaling Technology catalog #2280, RRID: AB_561245) overnight at 4°C. Membranes were then incubated with horseradish peroxidase-conjugated anti-rabbit IgGs (1/20000; Jackson ImmunoResearch Laboratories) for 1.5 h at room temperature. Immunoreactive bands were detected by enhanced chemiluminescence plus (PerkinElmer). Membranes were next stripped with buffer containing 0.2 M glycine pH 2.2, 0.1% SDS and reprobed with antibodies detecting level of total S6 (1/2000; Cell Signaling Technology catalog #2217 also 2217L, 2217S, RRID:AB_331355) and/or tubulin (1/1000; Cell Signaling Technology catalog #2148, RRID:AB_2288042) overnight at 4°C. All immunoreactive bands were scanned with a desktop scanner and quantified using Quantity One software (Bio-Rad).

Acute hippocampal slice preparation. Acute slices were prepared from 7- to 10-week -old Som-Raptor-WT and Som-Raptor-KO mice. Animals were anesthetized with isoflurane inhalation and the brain was rapidly removed and placed in ice-cold sucrose-based cutting solution containing the following (in mM): 75 sucrose, 87 NaCl, 2.5 KCl, 1.25 NaH_2PO_4, 7 $MgSO_4$, 0.5 $CaCl_2$, 25 $NaHCO_3$, 25 glucose, 11.6 ascorbic acid and 3.1 pyruvic acid, pH 7.4, and 295 mOsmol/L. A block of tissue containing the hippocampus was prepared and 300 or 400 μm (for whole-cell and field recordings, respectively) transverse hippocampal slices were cut with a Leica VT1000S vibratome. Slices were transferred for recovery for 30 min to a holding chamber in artificial CSF (ACSF) containing the following (in mM): 124 NaCl, 2.5 KCl, 1.25 NaH_2PO_4, 1.3 $MgSO_4$ 2.5 $CaCl_2$, 26 $NaHCO_3$, and 10 glucose (pH 7.3–7.4, 295–305 mOsmol/L) at 30°C and subsequently maintained at room temperature (20–22°C) for at least 90 min until use. Both cutting solution and ACSF were saturated with 95% O_2/5% CO_2.

Whole-cell recordings. For experiments in cultured slices, culture plate inserts were transferred to ACSF containing the following (in mM): 124 NaCl, 2.5 KCl, 1.25 NaH_2PO_4, 4 $MgSO_4$ 4 $CaCl_2$, 26 $NaHCO_3$, and 10 glucose (pH 7.3–7.4, 295–305 mOsmol/L) maintained at room temperature for at least 30 min until use. Acute and cultured slices were transferred to a submersion chamber perfused (3–4 ml/min) with ACSF at 31 ± 0.5°C, CA1 and CA3 regions were disconnected by a surgical cut and slices kept for an additional 30 min submerged before recording. EYFP-expressing CA1 interneurons were identified using an upright microscope (Nikon Eclipse, E600FN), equipped with a water-immersion long-working distance objective (40×, Nomarski Optics), epifluorescence and an infrared video camera. Whole-cell voltage-clamp recordings were obtained using borosilicate glass pipettes (2–5 MΩ; WPI) filled with intracellular solution containing the following (in mM): 120 $CsMeSO_3$, 5 CsCl, 2 $MgCl_2$, 10 HEPES, 0.5 EGTA, 10 Na_2-phosphocreatine, 2 ATP-Tris, 0.4 GTP-Tris, 0.1 spermine, 2 QX314, and 0.1% biocytin, pH 7.2–7.3, and 280 ± 5 mOsmol. For whole-cell current-clamp recordings, the intracellular solution contained the following (in mM): 120 $KMeSO_4$, 10 KCl, 10 HEPES, 0.5 EGTA, 10 Na_2-phosphocreatine, 2.5 MgATP, 0.3 NaGTP, and 0.1% biocytin (pH 7.4, 300 mOsmol/L). Data were acquired using a Multiclamp 700B amplifier (Molecular Devices), digitized at 20 kHz using Digidata 1440A and pClamp 10 (Molecular Devices). Recordings were low-pass filtered at 2 kHz. Access resistance was regularly monitored during experiments and data were included only if the holding current was stable and access resistance varied <20% of initial value. EPSCs were recorded in the presence of (2R)-amino-5-phosphonovaleric acid (AP5; 50 μM, Sigma-Aldrich) and SR-95531 (gabazine, 5 μM; Sigma-Aldrich) to block NMDA and $GABA_A$ receptors, respectively. Data were acquired and analyzed by an experimenter blinded for the genotype and the treatment of the animals.

Spontaneous EPSCs were recorded in voltage-clamp mode over a period of 1–5 min and 300 consecutive EPSCs analyzed for frequency and amplitude (MiniAnalysis; Synaptosoft). Evoked EPSCs were elicited using constant current pulses (50 μs duration) via an ACSF-filled bipolar theta-glass electrode (Harvard Apparatus) positioned ~100 μm lateral to the recorded cell soma at the border between CA1 stratum oriens and the alveus. Putative single-fiber EPSCs were evoked at 0.5 Hz using minimal stimulation (success rate = 40–50%). EPSC potency (EPSC amplitude excluding failures) was averaged over a 10–15 min period (pClamp 10). Because the failure rate was an adjusted parameter, we used EPSC potency to characterize amplitude changes in evoked transmission. Input-output function was studied by delivering current pulses of incremental intensity (0–600 μA, 50 μA steps); 3–10 trials per pulse intensity were delivered and responses averaged (including failures) to determine EPSC amplitude (initial EPSC peak). Linear regressions were applied on individual averaged responses; the slope (synaptic gain) and *x*-intercept (minimal stimulation intensity) of the linear regression of the input-output relationship were measured.

Membrane and firing properties of EYFP-labeled SOM interneurons were measured in current-clamp recordings (Tricoire et al., 2011). Resting membrane potential was measured with the holding current I = 0 pA immediately after break-in. Input resistance (Rin) was measured using a linear regression of voltage deflections (± 15 mV max) in response to current steps (500 ms, 5 pA increment, holding membrane potential −60 mV), excluding responses with voltage deflections with activation of voltage-dependent conductance (voltage sag or ramps). Membrane time constant was calculated from the mean responses to 20 successive hyperpolarizing current pulses (−5 pA; 500 ms), determined by fitting voltage responses with a single exponential function and used to calculate specific membrane capacitance. Action potential (AP) threshold was taken as the voltage at which the slope trajectory reached 10 mV/ms. AP amplitude was the difference in membrane potential between threshold and peak. AP half-width was calculated as AP duration at half-amplitude. Fast afterhyperpolarization (fAHP) amplitude was calculated as the difference between threshold and the negative peak after the AP. The time difference between the current pulse onset and the AP peak was defined as AP latency. The rheobase was measured as the minimal current amplitude necessary to evoke an action potential. AP properties were mea-

sured for the first AP elicited by a 500 ms depolarizing current pulse just sufficient to reach threshold. The sag index was determined from a series of negative current steps (500 ms duration, 10 pA steps). From the V–I plots, the peak negative voltage deflection (Vhyp) and the steady-state voltage deflection (Vsag, calculated for the last 50 ms of the current step) were used to calculate the index as the ratio (Vrest − Vsag)/(Vrest − Vhyp), for current injections corresponding to Vsag = −80 mV.

Electrical stimulation protocol for late-LTP induction. Late-LTP was induced by electrical stimulation in acute slices using a concentric bipolar Pt/Ir electrode (FHC, Bowdoin, ME) positioned in the stratum oriens close to the alveus. Late-LTP induction protocol consisted of 4 trains of theta-burst stimulations (TBS) at 5 min intervals. Each TBS train consisted of 3 episodes (at 30 s intervals) of 5 bursts (at 250 ms interburst intervals) of 4 pulses at 100 Hz (Perez et al., 2001; Vasuta et al., 2015). Whole-cell recordings were obtained from EYFP-positive interneurons located ~100 μm lateral to the stimulating electrode at 2 h after late-LTP induction or after a similar period in unstimulated slices. LTP was assessed by recording EPSCs evoked by minimal stimulation through an ACSF-filled bipolar theta-glass electrode positioned at approximately the same site as the stimulating electrode used for LTP induction.

Field recordings. Field EPSPs (fEPSPs) were recorded as previously (Vasuta et al., 2015) in CA1 stratum radiatum with glass electrodes (1–3 MΩ; WPI) filled with ASCF. Schaffer collaterals were stimulated (0.1 ms duration; 30 s-1) using a concentric bipolar Pt/Ir stimulating electrode (FHC) placed in stratum radiatum proximal to the CA3 region. A second concentric bipolar Pt/Ir stimulating electrode was positioned in the oriens/alveus border proximal to the subiculum for theta-burst conditioning trains (as described above). Field potentials were recorded with a differential extracellular amplifier (Microelectrode AC Amplifier Model 1800, A-M Systems), filtered at 2 kHz, digitized at 10 kHz (Digidata 1440A), and analyzed with pClamp10 (Molecular Devices). Stimulus intensity was adjusted to elicit 35% of maximal fEPSP. Basal synaptic transmission was assessed by recording fEPSP in response to incremental stimulations (20 to 180 μA, 20 μA steps). Short term plasticity was assessed by fEPSP in response to paired-pulse stimulations with incremental delays (20 to 110 ms, 30 ms steps). LTP was induced at CA1 Schaffer collateral synapses through the stimulating electrode in the stratum radiatum by a weak high-frequency stimulation train (wHFS; 750 ms, 100 Hz) (Vasuta et al., 2015). Two hours before LTP induction in the Schaffer collateral pathway, the conditioning TBS protocol to induce late-LTP in SOM interneurons (as described above) was applied at the oriens/alveus border. fEPSP slope was measured at 10–90% of fEPSP amplitude.

Confocal imaging and cell reconstruction. Neurons were labeled with 0.1% biocytin added to the whole-cell patch pipette internal solution. At the end of experiments, hippocampal slices were postfixed overnight at room temperature in 4% paraformaldehyde in 0.1 M phosphate buffer and 0.1% Triton. The morphology of stained neurons was revealed using 1/1000 cy3-conjugated streptavidin (Rockland Immunochemical) incubated overnight at room temperature. Cy3 was excited at 543 nm wavelength and images were captured using an LSM 880 confocal microscope (Zeiss). Stack images (1 μm steps) were acquired through a 40× water-immersion objective to perform three-dimension reconstructions and Sholl analysis of SOM interneurons using the Simple Neurite Tracer and Sholl Analysis Fiji plugins (ImageJ). SOM interneuron reconstructions revealed that in each group (Som-Raptor-WT and Som-Raptor-KO mice), 90% displayed all features of OLM type of SOM interneurons, the remaining 10% showing dense axonal arborization in strata oriens and radiatum, typical of bistratified cells or axonal collateral running out from the hippocampus typical of projection cells (Pelkey et al., 2017).

Behavioral experiments. Before behavioral experiments, mice were gently handled daily for 3 d (~1 min per mouse) to habituate mice to the experimenter and reduce the stress related to the experimental handling. Mice were 8–13 weeks old. The experimenter was blind to the genotype of the mice. In all experiments, mice were first video-tracked at 25 frames/s and their movements subsequently analyzed using a position tracking system (Smart 3.0; PanLab). Mice performed the open-field test first; the Barnes maze test started the next day and the fear conditioning occurred 5 d after the end of the Barnes maze session. Half of the mice were subjected to fear conditioning only.

Open-field test. Mice were allowed to freely explore a home-made circular (Som-Raptor-WT and Som-Raptor-KO mice, 60 cm diameter, 25 cm height) or square (Som-TSC1-WT and Som-TSC1-KO mice, PanLab) open-field for 5 min. Locomotion was evaluated by measuring the number of zone transitions using a pattern divided into 25 (circular OF) or 21 (squared OF) zones of equal size. Anxiety was assessed by measuring the time spent in a 20 cm radius/side central zone versus in a 20 cm broad peripheral annulus.

Fear conditioning. Mice were trained in conditioning chambers that were housed in sound- and light-isolated cubicles (Coulbourn Instruments). The chambers contained a stainless steel grid floor, overhead LED lighting, camera and were supplied with background noise (60 dB) by an air extractor fan. The experimental protocol was based on Ruediger and coworkers (Ruediger et al., 2011) with slight modifications. The training context was rectangular with transparent walls and was cleaned with 1% acetic acid before and after each trial. Two neutral contexts were designed to assess contextual generalization and discrimination. One had a triangular shape, transparent walls and was cleaned with 70% ethanol before and after each trial. This context was considered novel but similar to the training context because they shared some features. Another neutral context had a circular shape, opaque black and reflective walls, Plexiglas floor and was cleaned with 70% ethanol before and after each trial. This context was considered novel and distinct to the training context. Freezing was assessed using FreezeFrame (Coulbourn Instruments). Once placed in the conditioning chamber, mice were allowed to freely explore for 2.5 min, and then received 5 presentations of unconditioned and conditioned stimuli (1 s foot shock, 0.8 mA; where indicated, 10 kHz tone for 10 s, 70 dB sound pressure level, 30 s interleaved). The last 1 s of each tone was paired with the unconditioned stimulus. To test for cued fear conditioning, mice explored the novel distinct context for 2.5 min, followed by 5 tone presentations (tone-dependent freezing). Contextual fear conditioning involved the same protocol, but without the tone component. To test for contextual fear memory, mice were returned to the training context during a test period of 2.5 min, at 1 or 24 h after conditioning, to assess short- or long-term memory, respectively. To test for contextual discrimination after fear conditioning, a within-subjects design was used. On the test day, 5 h after the test in the training context, mice were pseudorandomly distributed across the two novel neutral contexts and freezing was assessed during 2.5 min. Discrimination ratio was calculated as the amount of freezing in (training context)/(training context + novel context) (Wiltgen and Silva, 2007). A ratio of 1 indicates that mice were able to discriminate the contexts perfectly, and a ratio of 0.5 means that they were unable to discriminate. For a subset of training-induced persistent plasticity experiments, mice were subjected to contextual fear conditioning 30 min after IP injection of 1 mg/kg JNJ16259685 (Tocris Bioscience) or vehicle.

Barnes maze. This test was used to assess hippocampus-dependent spatial learning (Barnes, 1979) using an elevated platform (PanLab). The experimental protocol was based on Sunyer and coworkers (Sunyer et al., 2007) with slight modifications. Mice were trained to use spatial cues to find a small dark escape chamber under the platform termed "target." The target is retained at the same position relative to the room, while the platform is rotated with each trial to discourage use of the intramaze odor cues. In addition, the platform, the starting chamber and the escape box were thoroughly cleaned (Versaclean 10%) between every single trial to reduce any possible scent trails. Assignment of target location was balanced among experimental groups. An aversive pulsed noise (85 dB) went on during each trial and switched off when the mouse entered in the target. One day after a familiarization period (day 1), mice were trained in 4 daily sessions with an intertrial interval of 15 min for 4 d. During the training, mice were left 10 s in a dark cylinder (starting chamber) in the center of the maze, allowed to freely explore the maze for a maximum duration of 3 min and left 1 min in the escape box after each trial. If a mouse failed to find the target by the end of the 3 min period, it was gently guided to it. Video tracking and data analysis were performed using Smart 3.0 (PanLab). On day 6, the mice were exposed to a probe trial in which the escape box was closed. Mice were allowed to explore the maze for 3 min. The number of errors, the latency and the distance traveled before the first reaching of the target (primary search) were collected.

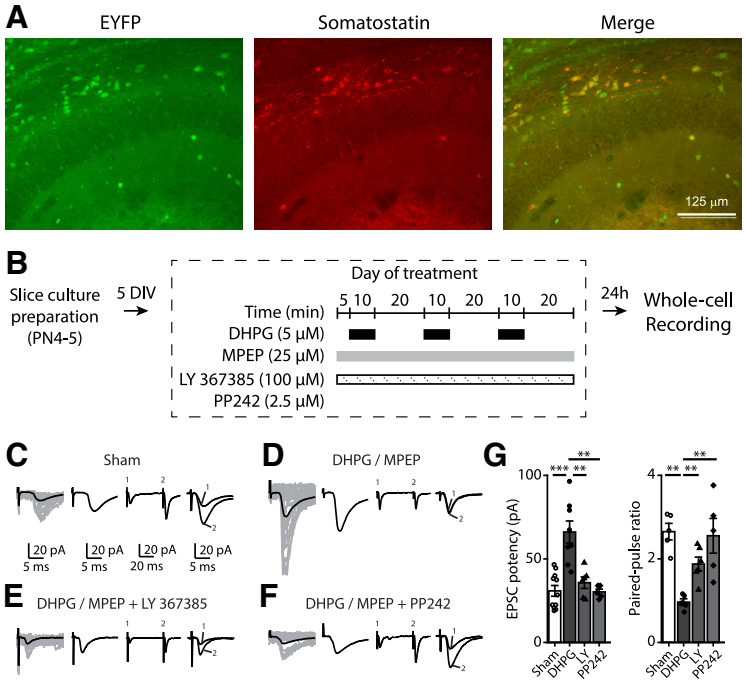

Figure 1. Chemically induced persistent LTP at excitatory synapses onto CA1 SOM-INs depends on mGluR1a and mTOR. ***A***, Representative images of EYFP expression (left) and SOM immunofluorescence (middle) in hippocampal CA1 area from $Sst^{ires\text{-}Cre}$;$Rosa26^{lsl\text{-}EYFP}$ mice, showing 84.4 ± 2.6% of EYFP+ cells colabeled for somatostatin (right) in stratum oriens. ***B***, Diagram of chemical late LTP induction and recording protocol in organotypic slice cultures. ***C–F***, Representative EPSCs evoked by minimal stimulation in EYFP expressing SOM-INs at 24 h after induction in different conditions: sham treatment (***C***), and repeated mGluR1 stimulation alone (***D***), in the presence of the mGluR1a antagonist LY367385 (***E***) or mTOR inhibitor PP242 (***F***). From left to right: EPSCs including failures (individual traces in gray, average trace in black), averaged EPSC potency (excluding failures), average of EPSCs evoked by paired-pulse stimulation, and superimposed first and second EPSCs of average pair. ***G***, EPSC potency (EPSC amplitude excluding failures) and paired-pulse ratio after sham and MPEP/DHPG alone, in the presence of LY367385 or PP242. $^{**}p < 0.01$; $^{***}p < 0.001$

During the total search (90 s), the time spent in the quadrants (target, left, right and opposite, excluding a 15 cm diameter central zone) and the number of visits for each hole were collected. Nontarget data were defined as the average number of visits in the 19 nontarget holes. The selective search ratio was defined as the number of visits in (target)/(target + nontarget). A ratio of 1 indicates that a mouse visited only the target hole, and a ratio of 0.5 means that it visited target and nontarget holes equally. Search strategies were also collected and defined into three categories: (1) direct (spatial), moving directly to the target hole or to an adjacent hole before visiting the target; (2) serial (thygmotactism), the first visit to the target hole preceded by visiting at least two adjacent holes in serial manner in a clockwise or counterclockwise direction; and (3) random (or mixed), hole searches separated by crossing through the center of the maze or unorganized search (Barnes, 1979; Fox et al., 1998). One search strategy was attributed for every single trial of the training and for the primary search of the probe test.

The two sets of experiments with Som-Raptor-KO and Som-TSC1-KO mice were performed in two different rooms, with two distinct settings, at different periods, and by two different experimenters, likely accounting for differences in the WT strains in the Barnes maze experiments.

Statistical analysis. No statistical methods were used to predetermine the sample size, but our sample sizes are similar to (or larger than) those generally used in the field. Statistical analysis was performed using OriginPro 2016 (OriginLab). Data were tested for normality and homoscedasticity using the Shapiro–Wilk and the Brown–Forsythe tests, respectively. We used Student's *t* tests (with Welch corrections for heteroscedasticity), two-way ANOVA with Tukey's pairwise comparison tests (with Bonferroni adjustments for multiple comparisons), and two-way repeated-measures ANOVA when data passed normality and homoscedasticity assumptions. Mann–Whitney tests and Friedman ANOVA were used when it was not the case. All the tests were two-sided. In the figures, data are expressed as arithmetic mean ± SEM. Asterisks denote statistical significance as calculated by the specified statistical tests ($^{*}p < 0.05$; $^{**}p < 0.01$; $^{***}p < 0.001$; ns, not significant).

Results

We first established that mGluR1a- and mTORC1-dependent late-LTP (Ran et al., 2009, 2012) occurs at excitatory synapses onto CA1 SOM-INs in mice expressing EYFP under the control of the SOM promoter ($Sst^{ires\text{-}Cre}$;$Rosa26^{lsl\text{-}EYFP}$). As previously reported for mature hippocampus (Vasuta et al., 2015), the vast majority of CA1 EYFP-expressing interneurons in slice cultures from $Sst^{ires\text{-}Cre}$;$Rosa26^{lsl\text{-}EYFP}$ mice were immunopositive for SOM and located in stratum oriens (Fig. 1*A*). Whole-cell recordings from CA1 EYFP-expressing SOM-INs revealed that EPSCs were potentiated at 24 h after repeated chemical mGluR1 stimulation (Fig. 1*B*). EPSC potency was increased (Kruskal–Wallis ANOVA, $p = 0.0004$, Mann–Whitney test, sham, $n = 11$, vs DHPG, $n = 8$: $p = 0.0008$), and paired-pulse ratio (PPR) was decreased (Kruskal–Wallis ANOVA, $p = 0.006$, Mann–Whitney test, sham vs DHPG: $p = 0.008$), compared with sham treated slices (Fig. 1*C*,*D*,*G*). EPSC potentiation was prevented by the mGluR1a antagonist LY367385 ($n = 6$; Mann–Whitney tests, potency: $p = 0.006$; PPR: $p = 0.005$; Fig. 1*E*,*G*) or the mTOR inhibitor PP242 ($n = 5$; Mann–Whitney tests, potency: $p = 0.004$; PPR: $p = 0.008$; Fig. 1*F*,*G*). Therefore, persistent late-LTP occurs at synapses onto SOM-INs and is dependent on mGluR1a and mTOR signaling.

Cell-specific *Rptor* deletion prevents mTORC1 signaling in SOM-INs

mTORC1 is a key regulator of translation in long-term synaptic plasticity (Costa-Mattioli et al., 2009; Ran et al., 2009). We investigated specifically the role of mTORC1 in SOM-INs in transgenic mice with a cell-specific homozygous knock-out of *Rptor* in SOM-INs ($Sst^{ires\text{-}Cre}$;$Rosa26^{lsl\text{-}EYFP}$;$Rptor^{fl/fl}$ mice, termed Som-Raptor-KO) and wild-type control mice ($Sst^{ires\text{-}Cre}$;$Rosa26^{lsl\text{-}EYFP}$;$Rptor^{WT/WT}$, termed Som-Raptor-WT). First we characterized the loss of mTORC1 function in SOM-INs in these mutant mice. The number of CA1 EYFP-expressing SOM-INs immunopositive for Raptor was drastically reduced in Som-Raptor-KO mice compared with Som-Raptor-WT, confirming a Raptor expression deficit in SOM-INs (WT: $n = 7$, KO: $n = 8$; Mann–Whitney test, $p = 0.0013$; Fig. 2*A*). Next we confirmed the cell-type selectivity of *Rptor* deletion. Western blots assays of Raptor in hippocampal lysates (Fig. 2*B*) and cultured slices (Fig. 2*C*) showed no difference in total hippocampal Raptor and p-S6 expression in lysates (Raptor: WT: $n = 6$, KO: $n = 6$; $t_{10} = -0.8$, $p = 0.44$; p-$S6^{S235/236}$: WT: $n = 3$, KO: $n = 3$; $t_4 = -0.3$, $p = 0.81$) and cultured slices (Raptor: WT: $n = 2$, KO: $n = 2$; Mann–Whitney, $p = 1$; p-$S6^{S235/236}$: WT: $n = 3$, KO: $n = 3$; $t_2 = -0.8$, $p = 0.49$) in Som-Raptor-KO and Som-Raptor-WT mice, indicating that hip-

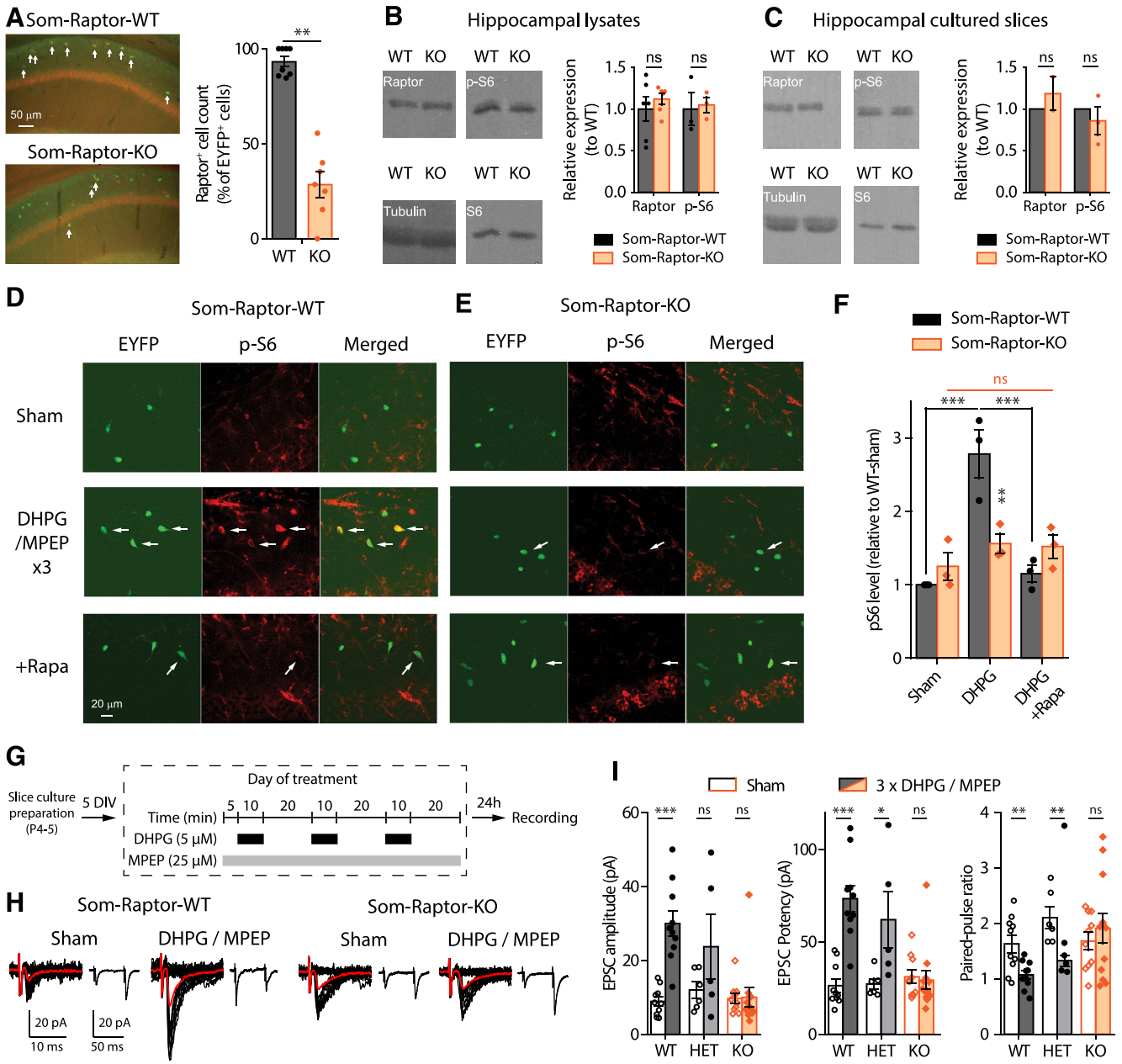

Figure 2. Cell-specific deficit in Raptor expression impairs mTORC1 signaling and late-LTP in SOM-INs of Som-Raptor-KO mice. ***A***, Left, Representative images of Raptor immunopositive (red) EYFP$^+$ (green) CA1 SOM-INs (arrows, colabeling) in Som-Raptor-KO relative to Som-Raptor-WT mice. Right, Percentage of Raptor$^+$ cells relative to EYFP$^+$ cells. ***B***, Left, Representative Western blots of Raptor and phospho-S6$^{S235/236}$ from hippocampal lysates. Right, Raptor (normalized to tubulin) and p-S6 (normalized to S6 and tubulin) levels (relative to Som-Raptor-WT mice). ***C***, Same as in (***B***) but in hippocampal cultured slices. ***D***, ***E***, Representative confocal images illustrating EYFP$^+$ CA1 SOM-INs (green), S6$^{S235/236}$ phosphorylation (red) and colabeling (merged) in Som-Raptor-WT (***D***) and Som-Raptor-KO (***E***) mice, after sham, DHPG/MPEP and DHPG/MPEP in the presence of 1 μM rapamycin treatments. Arrows point to EYFP$^+$ SOM-INs with p-S6 colabeling. ***F***, Phosphorylated S6$^{S235/236}$ level relative to sham treatment in Som-Raptor-WT mice. ***G***, Diagram of chemical late-LTP experimental protocol in cultured slices. ***H***, Representative EPSCs evoked by minimal stimulation in SOM-INs. Traces are superimposed 20 consecutive events (EPSCs + failures, black), average EPSC (including failures, red) and average of EPSC pairs (20 events) evoked by paired-pulse stimulation. ***I***, EPSC amplitude (including failures), EPSC potency (excluding failures) and paired-pulse ratio of SOM-INs 24 h after DHPG/MPEP relative to sham treatment in Som-Raptor-WT, Som-Raptor-HET, and Som-Raptor-KO mice. *$p < 0.05$; **$p < 0.01$; ***$p < 0.001$; ns, not significant.

pocampal principal neurons are unaffected by conditional deletion of *Rptor* in SOM-INs.

We then verified impairment of mTORC1 signaling in SOM-INs using immunofluorescence (Ran et al., 2009). Repeated mGluR1 stimulation in hippocampal slices of Som-Raptor-WT mice increased phosphorylation of ribosomal S6 protein, a downstream effector of mTORC1, in SOM-INs, and this effect was prevented by the mTORC1 inhibitor rapamycin (Fig. 2*D*,*F*). Repeated mGluR1 stimulation failed to increase S6 phosphorylation in SOM-INs in Som-Raptor-KO mice, confirming the loss of mTORC1 signaling (Fig. 2*E*,*F*; two-way ANOVA, $F_{(2,17\ \text{interaction})} = 11.6$, $p = 0.002$; Bonferroni's tests: WT-sham, $n = 3$, vs WT-DHPG, $n = 3$, $p = 0.0002$; WT-DHPG vs WT-DHPG+rapamycin, $n = 3$, $p = 0.0006$; KO-sham, $n = 3$, vs KO-DHPG, $n = 3$, $p = 1$; KO-DHPG vs KO-DHPG+rapamycin, $n = 3$, $p = 1$; WT-DHPG vs KO-DHPG, $p = 0.008$).

Next we assessed whether mTORC1-mediated late-LTP was affected in SOM-INs. In slice cultures of Som-Raptor-WT mice,

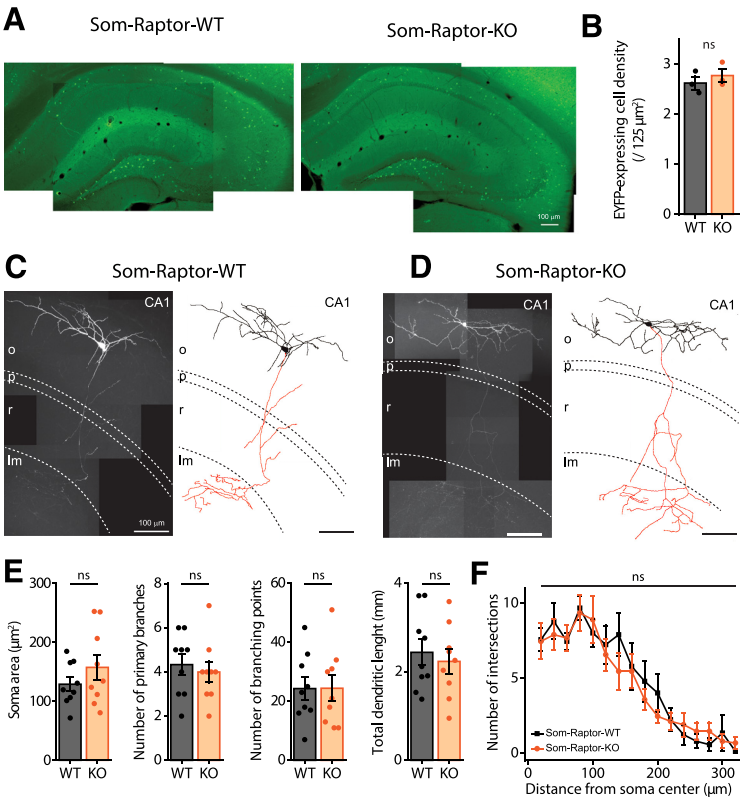

Figure 3. Intact SOM interneuron numbers and morphology in Som-Raptor-KO mice. ***A***, Montage of representative fluorescence images of EYFP expression in Som-Raptor-WT (left) and Som-Raptor-KO (right) mice. ***B***, EYFP-expressing cell density in CA1 of Som-Raptor-WT and Som-Raptor-KO mice. ***C***, ***D***, Montage of representative confocal images, maximum intensity *z*-projection (100 stacked images, 1 μm steps) of hippocampal CA1 SOM-IN filled with biocytin (left) and reconstructions (soma and dendrite in black, axon in red; right) from Som-Raptor-WT (***C***) and Som-Raptor-KO (***D***) mice. As illustrated, the vast majority (90%) of EYFP-expressing SOM-INs recorded in whole-cell and filled with biocytin in the present study corresponded to the O-LM type of SOM-INs (the remaining 10% corresponding to bistratified cells and projection cells). The dashed lines indicate the approximate boundaries of strata oriens (o), pyramidale (p), radiatum (r), and lacunosum/moleculare (lm). ***E***, Somatic and dendritic morphometric parameters of biocytin-filled SOM-INs in Som-Raptor-WT and Som-Raptor-KO mice. ***F***, Sholl analysis of dendritic arborization of reconstructed SOM-INs (20 μm bins) in Som-Raptor-WT and Som-Raptor-KO mice. ns, not significant.

repeated mGluR1 stimulation (Fig. 2*G*), increased amplitude (sham: $n = 10$, DHPG: $n = 10$; t test with Welch correction, $t_{11.2} = 5.8$, $p = 0.0001$) and potency (Mann–Whitney, WT: $p = 0.0003$), and reduced paired-pulse ratio (t test with Welch correction, $t_{13.2} = 3.2$, $p = 0.007$), of EPSCs in SOM-INs, relative to sham-treatment (Fig. 2*H*,*I*). Repeated mGluR1 stimulation failed to produce potentiation of EPSCs in Som-Raptor-KO mice (sham: $n = 12$, DHPG: $n = 10$; amplitude: Mann–Whitney tests, $p = 0.39$; potency: $p = 0.34$; paired-pulse ratio: t test with Welch correction, $t_{20} = -0.7$, $p = 0.48$), indicating a block of persistent plasticity at excitatory synapses onto SOM-INs (Fig. 2*H*,*I*). SOM-INs basal excitatory synaptic transmission was intact as EPSCs were similar in Som-Raptor-KO and Som-Raptor-WT mice in sham-treated conditions. Heterozygous Som-Raptor-KO (HET, sham: $n = 5$; MPEP/DHPG: $n = 6$) mice failed to show a deficit in late-LTP (EPSC amplitude: t test with Welch correction, $t_{4.5} = 1.3$, $p = 0.26$; potency: Mann–Whitney test, $p = 0.022$; PPR: $t_9 = 3.3$, $p = 0.009$; Fig. 2*I*). Together, these results show that conditional *Rptor* knock-out in SOM-INs results in deficient mTORC1-mediated signaling and synaptic plasticity in SOM-INs.

As control, we verified that the numbers of CA1 SOM-INs were unaffected in Som-Raptor-KO ($n = 3$ mice, 3 replicates each) relative to Som-Raptor-WT ($n = 3$ mice, 3 replicates each) mice ($t_4 = -0.8$, $p = 0.49$; Fig. 3*A*,*B*), indicating that *Rptor* deletion driven by the SOM promoter did not alter SOM-INs proliferation and migration. In addition, because mTORC1 is a key regulator of protein synthesis implicated in cell growth (Saxton and Sabatini, 2017), we used whole-cell current-clamp recordings and reconstruction of biocytin-filled SOM-INs in acute slices to assess general somatic and dendritic morphology, as well as basic membrane properties of CA1 SOM-INs in Som-Raptor-KO mice. Soma area ($t_{16} = 1.1$, $p = 0.27$), number of primary branches ($t_{16} = 0.3$, $p = 0.74$), number of branching points ($t_{16} = -0.3$, $p = 0.75$), total dendritic length ($t_{16} = -0.5$, $p = 0.60$) and the Sholl analysis of SOM-INs dendritic arborization (two-way RM ANOVA, $F_{(9,144\ \text{interaction})} = 0.6$, $p = 0.82$) were not different in Som-Raptor-WT ($n = 9$ cells in 5 mice) and Som-Raptor-KO ($n = 9$ cells in 5 mice) mice (Fig. 3*C*–*F*). Moreover, resting membrane potential (Mann–Whitney test, $p = 0.06$), input resistance (Mann–Whitney, $p = 0.51$), specific membrane capacitance (Mann–Whitney test, $p = 0.49$), sag index ($t_{26} = 0.3$, $p = 0.8$), latency to first AP (Mann–Whitney test, $p = 0.14$), rheobase (Mann–Whitney test, $p = 0.61$), AP amplitude ($t_{37} = -0.2$, $p = 0.81$) and adaptation ratio at rheobase $\times 4$ ($t_{35} = 2$, $p = 0.055$) were not changed in Som-Raptor-KO ($n = 14$–20 cells from 10 mice) relative to Som-Raptor-WT ($n = 14$–18 cells from 9 mice; Fig. 4). AP threshold (t test with Welch correction, $t_{24.7} = 3.1$, $p = 0.005$), AP half-width ($t_{37} = 2.2$, $p = 0.031$) and fAHP amplitude ($t_{37} = -2.7$, $p = 0.011$) were decreased and firing rate at rheobase $\times 2$ (Mann–Whitney test, $p = 0.0015$) was increased in Som-Raptor-KO compared with Som-Raptor-WT (Fig. 4). These results indicate deficits in mTORC1 signaling and synaptic plasticity, with relatively intact morphological and membrane properties, aside modest increase of intrinsic excitability, in SOM-INs of conditional KO mice.

SOM-IN specific *Rptor* deletion impairs hippocampus-dependent long-term memory

mTORC1 is a key regulator of translation in hippocampal long-term memory (Costa-Mattioli et al., 2009). Because hippocampal SOM-INs have been proposed to support contextual fear memories (Lovett-Barron et al., 2014; Schmid et al., 2016), we examined the consequences of impairment of SOM-IN mTORC1 function in hippocampus-dependent memory tasks. We first verified in the open-field test that Som-Raptor-KO mice showed normal anxiety level (Mann–Whitney tests, time in center: $p = 0.43$; periphery: $p = 0.1$; ratio: $p = 0.27$; Fig. 5*A*,*B*) and no impairment in locomotion, relative to Som-Raptor-WT mice (total distance traveled ($t_{52} = -2.8$, $p = 0.008$), zone transition number (Mann–Whitney test, $p = 0.002$), percentage of resting time ($t_{52} = 2.8$, $p = 0.007$) and running speed ($t_{52} = -1.9$, $p = 0.057$; $n = 27$ in each group; Fig. 5*A*,*C*). We next tested the mice in contextual fear learning and context discrimination (Fig. 5*D*).

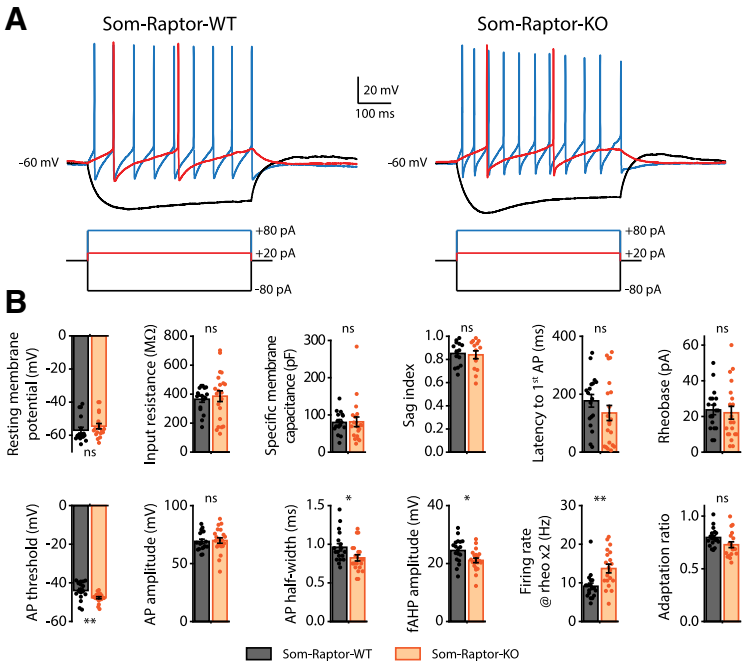

Figure 4. Membrane and firing properties of SOM-INs from Som-Raptor-KO mice. ***A***, Representative electrophysiological responses (top) of SOM-INs to current pulse injections (bottom) from Som-Raptor-WT (left) and Som-Raptor-KO (right) mice. Depolarizing current pulses correspond to near threshold (red) and 4 × threshold (blue) stimulation. ***B***, Membrane and firing properties of SOM-INs from Som-Raptor-WT and Som-Raptor-KO mice.*$p < 0.05$; **$p < 0.01$; ns, not significant.

Som-Raptor-KO and Som-Raptor-WT mice froze identically in response to foot shocks, indicating normal anxiety and sensorimotor gating (WT: $n = 55$, KO: $n = 51$; Mann–Whitney, $p > 0.05$; Fig. 5*E*). In the short-term memory test (1 h), Som-Raptor-KO and Som-Raptor-WT mice showed similar freezing (WT: $n = 11$, KO: $n = 10$; Mann–Whitney, $p = 0.70$; Fig. 5*F*), indicating intact short-term contextual fear memory. However, Som-Raptor-KO mice displayed reduced freezing compared with Som-Raptor-WT mice in the long-term memory test (24 h, WT: $n = 37$, KO: $n = 34$; $t_{69} = 4.12$, $p = 0.0001$; Fig. 5*F*), revealing a long-term contextual fear memory deficit. Mice were also tested for context discrimination in one of two novel contexts varying in similarity with the training context (Fig. 5*D*). When exposed to a novel context, Som-Raptor-WT mice froze more in the similar ($n = 13$) than in the distinct ($n = 13$) context (Mann–Whitney, $p = 0.0021$; Fig. 5*G*), manifesting context generalization and discrimination, respectively. Som-Raptor-KO mice showed reduced level of freezing in the similar novel context ($n = 14$) compared with Som-Raptor-WT mice (Mann–Whitney, $p = 0.0009$; Fig. 5*G*). Similar results were obtained using discrimination ratios to assess context discrimination normalized to the freezing level in the training context (two-way ANOVA, $F_{(1,47\ \text{interaction})} = 5.4$, $p = 0.024$; Tukey's tests, WT-similar vs WT-distinct: $p = 0.03$; KO-similar vs KO-distinct: $p = 0.96$; WT-similar vs KO-similar: $p = 0.003$; WT-distinct vs KO-distinct: $p = 0.50$; Fig. 5*G*). Because Som-Raptor-KO mice did show reduced but still substantive freezing in the training context compared with the WT mice, this increased discrimination ratio in the similar context suggests alteration in context generalization.

Fear conditioning strongly relies on amygdala function, where SOM-INs play crucial roles (Li et al., 2013; Penzo et al., 2015). We subjected mice to auditory-cued fear conditioning (Fig. 5*H*), a task that does not engage dorsal hippocampus, to assess whether conditional *Rptor* deletion in SOM-INs affected amygdala function. Som-Raptor-KO and Som-Raptor-WT mice showed similar levels of freezing in response to tone-shock presentations (WT: $n = 16$, KO: $n = 15$; Mann–Whitney, $p > 0.05$) and in the long-term memory probe test (Mann–Whitney, pre-tone and post-tone: $p = 0.57$; Fig. 5*I*), indicating that *Rptor* deletion in SOM-INs did not affect dorsal hippocampus-independent cued fear memory.

To investigate further the behavioral role of mTORC1 in SOM-INs, we examined spatial reference memory in the Barnes maze, a hippocampus-dependent spatial learning and memory task (Fig. 6*A*). Som-Raptor-WT ($n = 16$) and Som-Raptor-KO ($n = 15$) mice performed similarly during acquisition (errors: Friedman ANOVA, WT: $p = 0.0008$; KO: $p = 0.036$ and Mann–Whitney tests: S1: $p = 0.75$, S2: $p = 0.87$, S3: $p = 0.71$, S4: $p = 0.08$; latency: Friedman ANOVA, WT and KO: $p < 0.0001$ and Mann–Whitney tests: S1: $p = 0.89$, S2: $p = 0.78$, S3: $p = 0.86$, S4: $p = 0.013$; distance: repeated-measures ANOVA, $F_{(3,29\ \text{session})} = 16.2$, $p < 0.0001$; $F_{(1,29\ \text{genotype})} = 1.5$, $p = 0.23$; $F_{(3,29\ \text{interaction})} = 0.7$, $p = 0.53$), indicating intact spatial learning (Fig. 6*B*,*C*). During the memory probe test, Som-Raptor-KO mice performed poorly with increased number of errors (Mann–Whitney, $p = 0.017$), latency ($p = 0.007$) and traveled distance ($p = 0.005$) in the primary search for the target, indicating a deficit in long-term spatial memory at the single trial level, relative to Som-Raptor-WT mice (Fig. 6*B*,*D*). During the total search period, Som-Raptor-KO mice spent less time in the target quadrant than Som-Raptor-WT mice (two-way ANOVA, $F_{(3,116\ \text{interaction})} = 5.4$, $p = 0.002$ and Tukey's tests, WT-target vs KO-target: $p = 0.028$; Fig. 6*B*,*E*), indicating again an impairment in long-term spatial memory. In addition, Som-Raptor-KO mice visited less the target hole, relative to Som-Raptor-WT mice, demonstrating a deficit in spatial memory precision (visits: Wilcoxon tests, WT: $p = 0.0005$; KO: $p = 0.002$ and Mann–Whitney test, WT-target vs KO-target: $p = 0.007$; selective search ratio: t test against 0.5, WT: $t_{15} = 10.2$, $p < 0.0001$; KO: $t_{14} = 5.1$, $p = 0.0002$; WT vs KO: $t_{29} = 3.9$, $p = 0.0006$; Fig. 6*B*,*F*). Mice solve the Barnes maze using thygmotactic/serial and/or hippocampus-dependent spatial strategies (Barnes, 1979; Fox et al., 1998). During the training protocol, Som-Raptor-WT mice rapidly manifested thygmotactic behaviors to solve the task, visiting holes in a serial manner but progressively adopted a spatial strategy, navigating directly to the target hole (Cochran test, $p = 0.015$; $n = 16$ WT and 15 KO mice; Fig. 6*B*,*G*,*H*). Som-Raptor-KO mice did not significantly use spatial strategy but solved the maze by relying mostly on thygmotactic or mixed strategies (Cochran test, $p = 0.67$, WT: $n = 256$ total trials, KO: $n = 240$; z-score WT vs KO: $p = 0.016$; Fig. 6*B*,*G*,*H*), indicating an impairment in hippocampus-dependent spatial memory. Together, these results reveal that mTORC1 activity in SOM-INs is necessary for intact long-term spatial and contextual fear memory.

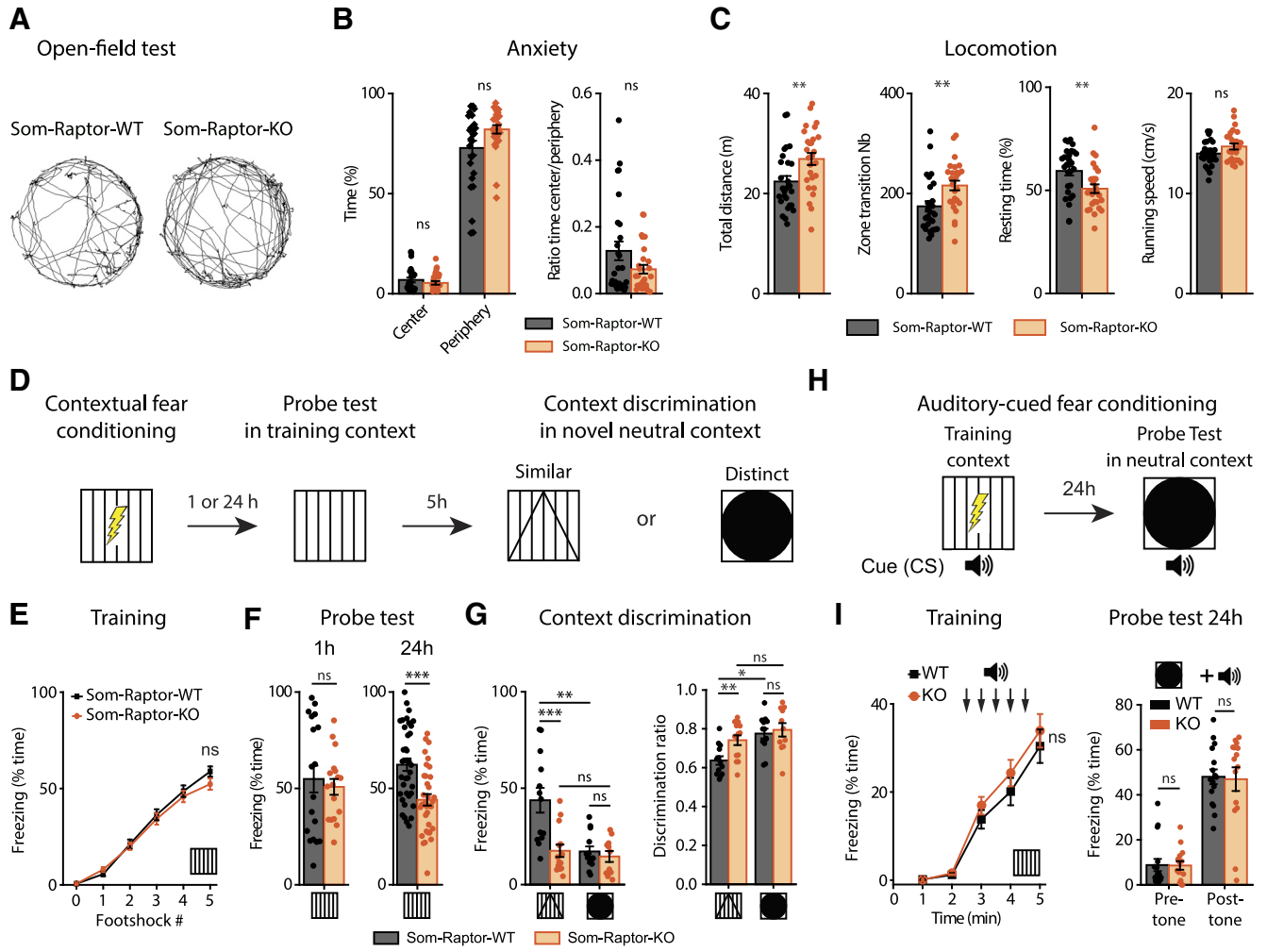

Figure 5. Som-Raptor-KO mice show impaired long-term contextual fear memory. ***A***, Representative paths traveled by Som-Raptor-WT (left) and Som-Raptor-KO (right) mice during 5 min free exploration in a circular open field. ***B***, Anxiety properties in the open-field test: percentage of time spent in the center and in the periphery (left) and center/periphery ratio (right). ***C***, Locomotion properties in the open-field test: total distance traveled, zone transition number, percentage of resting time and running speed. ***D***, Diagram of the contextual fear conditioning protocol. ***E***, Percentage of time freezing after each foot shock during the training session for Som-Raptor-WT and Som-Raptr-KO mice (0: before the first foot shock). ***F***, Percentage of time freezing during the probe tests at 1 h (left) and at 24 h (right). ***G***, Percentage of time freezing during the contextual discrimination test in a novel context (left) and discrimination ratio (right). ***H***, Diagram of the auditory-cued fear conditioning protocol. ***I***, Percentage of time freezing for Som-Raptor-WT and Som-Raptor-KO mice during the training session (left) and during the probe test at 24 h (right). $*p < 0.05$; $**p < 0.01$; $***p < 0.001$; ns, not significant.

Conditional *Tsc1* knock-down augments mTORC1 signaling in SOM-INs

Tuberous sclerosis complex (TSC) is a key negative regulator of mTORC1 under basal conditions and upstream signaling pathways inhibit TSC to activate mTORC1 (Saxton and Sabatini, 2017). We thus examined whether *Tsc1* knock-down in SOM-INs would be sufficient to upregulate mTORC1 activity and promote hippocampal memory. Hence we used transgenic mice with a cell-specific heterozygous knock-out of *Tsc1* in SOM-INs ($Sst^{ires\text{-}Cre}$;$Rosa26^{lsl\text{-}EYFP}$;$Tsc1^{WT/fl}$ mice, termed Som-TSC1-KO; and $Sst^{ires\text{-}Cre}$;$Rosa26^{lsl\text{-}EYFP}$; $Tsc1^{WT/WT}$, termed Som-TSC1-WT). We first confirmed the cell-type selectivity of *Tsc1* knock-out. Western blots assays showed no difference in phosphorylated S6 protein in hippocampal lysates in Som-TSC1-KO and Som-TSC1-WT mice (WT, $n = 12$, KO: $n = 13$; Mann–Whitney, $p = 0.25$; Fig. 7*B*), indicating unaffected mTORC1 signaling in hippocampal principal neurons. Using immunofluorescence, basal level of phosphorylation of ribosomal S6 protein was increased in SOM-INs in slices of Som-TSC1-KO mice relative to Som-TSC1-WT mice (WT, $n = 6$, KO: $n = 6$; $t_5 = 8.4$, $p = 0.0004$; Fig. 7*C–E*). Repeated mGluR1 (Fig. 7*A*) stimulation increased S6 phosphorylation in SOM-INs of Som-TSC1-WT relative to sham-treated ($t_5 = 3.2$, $p = 0.024$), but did not in Som-TSC1-KO mice (*t* test with Welch correction, $t_{6.1} = -0.8$, $p = 0.46$; Fig. 7*C–E*). Therefore, conditional *Tsc1* knock-down increased basal mTORC1 activity and occluded mGluR1-induced mTORC1 activation in SOM-INs.

We then determined the effect of *Tsc1* knock-down on chemically induced mTORC1-mediated late-LTP in SOM-INs (Fig. 7*A*). First, we found that basal synaptic transmission was unaffected in the mutant mice. In sham-treated slices, EPSC potency was unchanged in Som-TSC1-KO relative to Som-TSC1-WT mice (Fig. 7*F*,*G*). In acute slices of WT mice, like in cultured slices, repeated mGluR1 stimulation was necessary to induce persistent potentiation of EPSC potency, relative to sham treatment (Fig. 7*F*,*G*). However in slices of Som-TSC1-KO mice, a single mGluR1 stimulation was sufficient, but repeated treatment failed, to induce persistent potentiation of EPSC potency (two-way ANOVA, $F_{(2,71\ interaction)} = 19$, $p < 0.0001$, Bonferroni tests, WT-Sham, $n = 14$, vs WT-1xD, $n = 9$: $p = 0.99$, WT-Sham vs WT-3xD, $n = 16$: $p = 0.0014$, TSC1KO-Sham, $n = 14$,

vs TSC1KO-1xD, $n = 12$: $p = 0.0033$, TSC1KO-Sham vs TSC1KO-3xD, $n = 12$: $p = 0.98$; Fig. 7*F*,*G*), indicating a facilitation of induction of late-LTP in SOM-INs with *Tsc1* knock-down. We verified that SOM-IN chemical late-LTP in acute slices was mTORC1-mediated and found that persistent potentiation of EPSC potency by repeated mGluR1 stimulation was blocked in SOM-INs of Som-Raptor-KO mice (WT: $n = 9$, KO: $n = 10$; *t* test with Welch correction: $t_{12.7} = 0.5$, $p = 0.65$; Fig. 7*F*,*G*). We also found that rapamycin treatment prevented EPSC potentiation after a single mGluR1 stimulation in Som-TSC1-KO mice ($n = 7$; $t_{19} = 0.18$; $p = 0.86$; Fig. 7*G*), indicating a reversal of the electrophysiological abnormalities by rapamycin. Chemical late-LTP in acute slices was associated with unchanged paired-pulse ratio (WT vs TSC1, two-way ANOVA, $F_{(2,71\ \text{interaction})} = 0.3$, $p = 0.76$; TSC1KO-1xD vs TSC1KO-1xD+Rapamycin: *t* test with Welch correction: $t_{17,1} = -1.09$, $p = 0.29$; RaptorKO-Sham vs RaptorKO-3xD: *t* test with Welch correction: $t_{9.5} = 0.05$, $p = 0.96$; Fig. 7*F*,*G*), indicating some difference in mechanism with cultured slices.

Current-clamp electrophysiological characterization of SOM-INs in slices of Som-TSC1-KO mice showed no major difference in basic membrane properties (resting membrane potential: Mann–Whitney, $p = 0.35$; specific membrane capacitance: $t_{22} = -0.73$, $p = 0.47$; sag index: Mann–Whitney, $p = 0.12$) or firing (latency to first AP: $t_{22} = 1.4$, $p = 0.18$; rheobase: Mann–Whitney, $p = 0.27$; AP threshold: *t* test with Welch correction, $t_{18.6} = 0.1$, $p = 0.91$; AP amplitude: $t_{23} = 1.2$, $p = 0.23$; AP half-width: Mann–Whitney, $p = 0.08$; fAHP amplitude: $t_{22} = 1.2$, $p = 0.022$; firing rate at rheobase ×2: $t_{22} = 0.2$, $p = 0.84$ and adaptation ratio at rheobase ×3: $t_{19} = 0.5$, $p = 0.61$), except a reduction in input resistance (*t* test with Welch correction, $t_{11.5} = 2.7$, $p = 0.02$; $n = 10$–11 cells in 2 WT mice and 13–14 cells in 4 KO mice; Fig. 8).

Together, these results suggest that conditional mTORC1 upregulation in SOM-INs results in a lower threshold for induction of persistent synaptic plasticity in SOM-INs, and in an impairment of plasticity elicited by a normal induction paradigm, with largely intact intrinsic membrane properties.

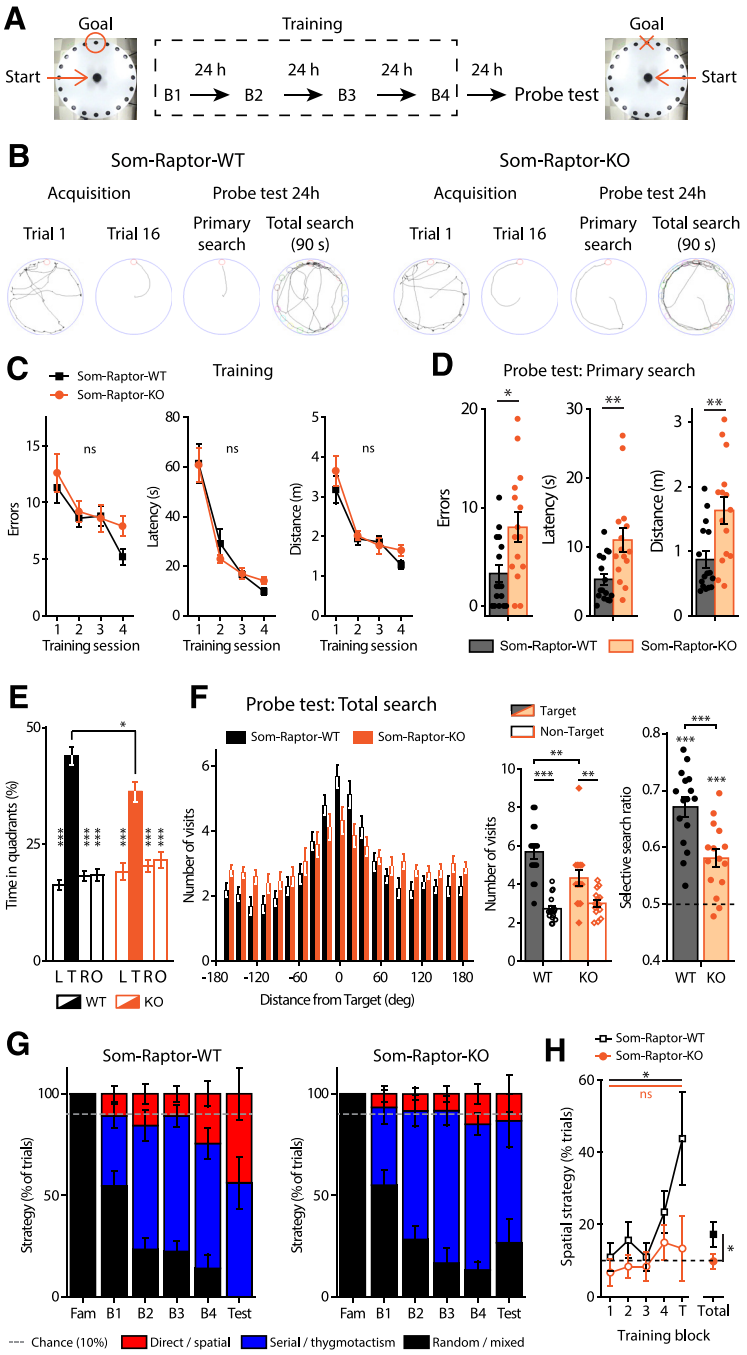

Figure 6. Som-Raptor-KO mice show impaired long-term reference spatial memory. ***A***, Diagram of the spatial learning protocol in the Barnes maze. ***B***, From left to right: representative paths traveled by Som-Raptor-WT (left) and Som-Raptor-KO (right) mice during the first and last (16th) acquisition trials, as well as during the primary search and total search of the probe test. ***C***, Performance in the Barnes maze during the training of Som-Raptor-WT and Som-Raptor-KO mice. ***D***, Spatial memory performance during the primary search of the probe test. Errors, latency and distance before the first visit of the target. ***E***, Percentage of time spent in each quadrant of the maze during the total search period of the probe test. L, Left, T, target; R, right; O, opposite quadrants. ***F***, Number of visits to all escape holes (left), number of visits expressed as target versus average of all nontarget holes (middle) and selective search ratios (right). ***G***, Percentage of total trials performed using one of three types of strategy (spatial, thygmotactism and random/mixed) to solve the maze by Som-Raptor-WT (left) and Som-Raptor-KO (right) mice. The dashed line represents chance level (10%) to find the target with a direct path. ***H***, Percentage of trials using a spatial strategy over the training protocol. The dashed line represents chance (10%). *$p < 0.05$; **$p < 0.01$; ***$p < 0.001$; ns, not significant.

Conditional *Tsc1* knock-down in SOM-INs augments hippocampus-dependent long-term memory

Next, we determined at the behavioral level the effects of *Tsc1* knock-down in SOM-INs. Som-TSC1-KO mice showed normal anxiety (Mann–Whitney tests, time in center: $p = 0.16$; periphery: $p = 0.84$; center/periphery ratio: $p = 0.22$; Fig. 9*A*,*B*) and slightly reduced locomotion (total distance traveled: Mann–Whitney test, $p = 3.5_{E}^{-5}$; number of zone transitions: $t_{36} = 5.4$,

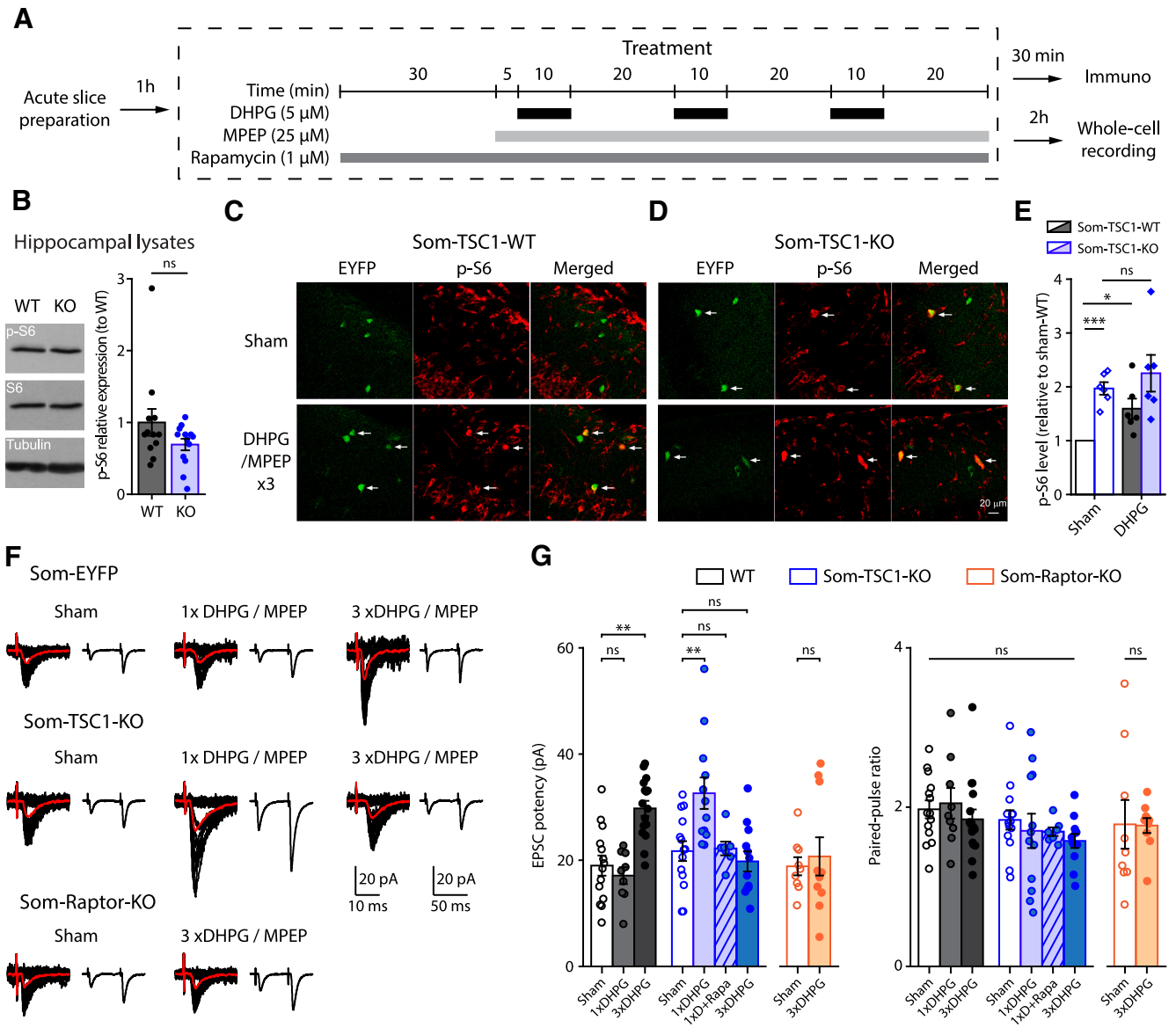

Figure 7. *Tsc1* knock-down increases mTORC1 signaling and facilitates mGluR1-mediated late-LTP in SOM-INs. ***A***, Diagram of chemical late-LTP experimental protocol in acute slices. ***B***, Left, representative Western blots of phosphorylated S6 $^{S235/236}$ from hippocampal lysates. Right, p-S6 $^{S235/236}$ (normalized to S6 and tubulin) levels (relative to Som-TSC1-WT mice). ***C***, ***D***, Representative confocal images illustrating EYFP $^{+}$ CA1 SOM-INs (green), S6 $^{S235/236}$ phosphorylation (red) and colabeling (merged) in Som-TSC1-WT (***C***) and Som-TSC1-KO (***D***) mice, after sham and DHPG/MPEP treatments. Arrows point to EYFP $^{+}$ SOM-INs with p-S6 colabeling. ***E***, p-S6 $^{S235/236}$ level in the different groups relative to sham treatment in Som-TSC1-WT mice. ***F***, Representative EPSCs evoked by minimal stimulation in SOM-INs. Traces are superimposed 20 consecutive events (EPSCs + failures, black), average EPSC (including failures, orange) and average of EPSC pairs (20 events) evoked by paired-pulse stimulation. ***G***, EPSC potency (excluding failures) and paired-pulse ratio of SOM-INs 2 h after sham, single and repeated DHPG/MPEP treatment in WT, Som-TSC1-KO and Som-Raptor-KO mice. *$p < 0.05$; **$p < 0.01$; ***$p < 0.001$; ns, not significant.

$p = 5.1_E{}^{-6}$; resting time: Mann–Whitney test, $p = 6.5_E{}^{-5}$; running speed: $t_{36} = 4.8$, $p = 3.1_E{}^{-5}$; Fig. 9*A*, *C*) in the open-field test (WT: $n = 17$, KO: $n = 21$). Then we examined contextual fear memory and context discrimination (Fig. 9*D*). Som-TSC1-KO and Som-TSC1-WT mice responded similarly to foot shocks (WT: $n = 28$, KO: $n = 31$; Mann–Whitney tests, $p > 0.05$; Fig. 9*E*), indicating intact sensorimotor gating. One hour after conditioning, Som-TSC1-KO and Som-TSC1-WT mice showed similar freezing (WT: $n = 12$, KO: $n = 13$; $t_{23} = -0.76$, $p = 0.46$; Fig. 9*F*), indicating intact short-term contextual fear memory. However, in the 24 h memory probe test, Som-TSC1-KO mice displayed increased freezing compared with Som-TSC1-WT mice (WT: $n = 16$, KO: $n = 18$; *t* test with Welch correction, $t_{22.2} = -3.08$, $p = 0.005$; Fig. 9*F*), revealing an augmentation of long-term contextual fear memory. When exposed to a novel distinct context, Som-TSC1-KO mice showed higher level of freezing (WT: $n = 8$, KO: $n = 8$; $t_{16} = 3.57$, $p = 0.0027$) and lower discrimination ratio ($t_{16} = 3.55$, $p = 0.003$) relative to Som-TSC1-WT mice, indicating impairment in context discrimination (Fig. 9*G*). These results suggest that increased mTORC1 activity in SOM-INs is sufficient to augment long-term contextual fear memory and generalization. Next, we examined whether amygdala function was affected. Som-TSC1-KO mice were subjected to auditory-cued fear conditioning (Fig. 9*H*) and showed no difference in freezing during the training (WT: $n = 11$, KO: $n = 13$; Mann–Whitney tests, $p > 0.05$; Fig. 9*I*) or 24 h memory probe test (Mann–Whitney, pre-tone: $p = 0.16$; post-tone: $p = 0.56$; Fig. 9*I*), indicating that upregulated mTORC1 activity in SOM-INs does not alter this dorsal hippocampus-independent memory task.

Finally, we investigated spatial memory performance of Som-TSC1-KO mice in the Barnes maze (Fig. 10*A*). Som-TSC1-KO mice showed fewer errors, shorter latency and traveled distance to target compared with WT during the acquisition (WT: $n = 21$, KO: $n = 23$; errors: repeated two-way ANOVA, $F_{(1,42\ \text{genotype})} = 9.47$, $p = 0.004$; latency: Friedman ANOVA, WT and KO: $p < 0.0001$ and Mann–Whitney tests, S1: $p = 0.26$, S2: $p = 0.012$, S3: $p = 0.0098$, S4: $p = 0.048$; distance: repeated two-way ANOVA, $F_{(1,42\ \text{genotype})} = 6.09$, $p = 0.018$; Fig. 10*B*,*C*) and the long-term memory test (Mann–Whitney tests, errors: $p = 0.0003$, latency: $p = 0.0009$; distance: $p = 0.002$; Fig. 10*B*,*D*), demonstrating better spatial learning and memory performance. During the total search period, Som-TSC1-KO mice visited more the target hole (Mann–Whitney, $p = 0.047$) and showed a higher selective search ratio than the Som-TSC1-WT mice (*t* test against 0.5, WT: $t_{20} = 4.61$, $p = 0.0002$; KO: $t_{22} = 9.76$, $p < 0.0001$; WT vs KO: $t_{42} = -2.91$, $p = 0.006$; Fig. 10*B*,*E*), indicating a better selective search of the target in Som-TSC1-KO mice.

These changes observed after *Tsc1* knock-down are the converse of changes found after *Rptor* deletion. Knock-down of *Tsc1* in SOM-INs upregulated mTORC1 activity and promoted hippocampal learning and memory. Therefore, mTORC1 activity level in SOM-INs appears to determine the level and contextual precision of hippocampal memories.

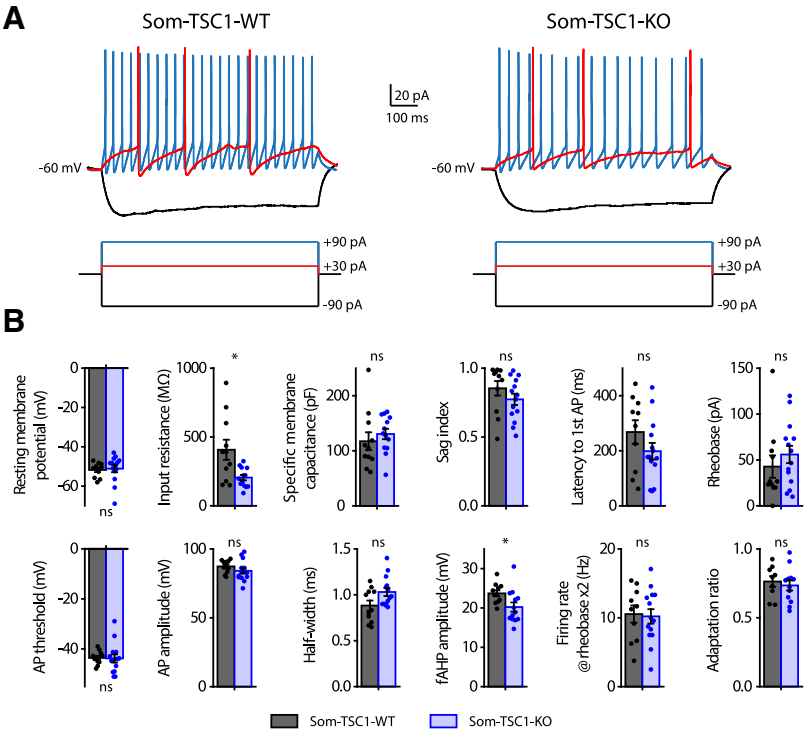

Figure 8. Membrane and firing properties of SOM-INs from Som-TSC1-KO mice. ***A***, Representative electrophysiological responses (top) of SOM-INs to current pulse injections (bottom) from Som-TSC1-WT (left) and Som-TSC1-KO (right) mice. Depolarizing current pulses correspond to near threshold (red) and 3× threshold (blue) stimulation. ***B***, Membrane and firing properties of SOM-INs from Som-TSC1-WT and Som-TSC1-KO mice, showing intact resting membrane potential, specific membrane capacitance, latency to first action potential (AP), rheobase, AP threshold, AP amplitude, AP half-width, firing rate at rheobase ×2 and adaptation ratio at rheobase ×3; and reduced input resistance and fAHP amplitude. *$p < 0.05$; ns, not significant.

Contextual fear learning induces mTORC1-mediated plasticity at SOM-IN excitatory synapses

Next we examined whether the effects of conditional genetic manipulations of mTORC1 on hippocampus-dependent memory and SOM-IN synaptic plasticity could be related. We tested whether contextual fear learning produces potentiation at SOM-INs excitatory synapses via mTORC1 using ex vivo whole-cell recordings in acute slices 24 h after training (Fig. 11*A*). SOM-INs from conditioned Som-Raptor-WT mice showed increased spontaneous EPSC frequency (naive: $n = 15$; CFC: $n = 13$; Mann–Whitney, $p = 0.015$) and amplitude (Fig. 11*B*,*C*), increased minimally evoked EPSC potency (naive: $n = 11$; CFC: $n = 14$; Mann–Whitney, $p = 0.0004$) associated with decreased minimal stimulation intensity and unchanged paired-pulse ratio (Fig. 11*D*,*E*), as well as potentiation of evoked EPSC input-output function (Fig. 11*F*,*G*), compared with naive mice. Therefore, conditioning induces potentiation of excitatory synapses onto SOM-INs lasting 24 h. The learning-induced potentiation was mTORC1-dependent. At 24 h posttraining, SOM-INs of Som-Raptor-KO mice failed to show any potentiation of EPSCs relative to naive mice (spontaneous EPSC amplitude: naive: $n = 11$; CFC: $n = 14$; two-way ANOVA, $F_{(1,49\ \text{interaction})} = 5.1$, $p = 0.004$; Tukey's tests, WT-naive vs WT-CFC, $p = 0.007$; KO-naive vs KO-CFC, $p = 0.69$; WT-naive vs KO-naive: $p = 1$; minimally evoked EPSC potency: KO-naive, $n = 10$, vs KO-CFC, $n = 12$: $p = 0.87$; paired-pulse ratio: two-way ANOVA, $F_{(1,43\ \text{interaction})} = 1.6$, $p = 0.22$; minimal stimulation intensity: two-way ANOVA, $F_{(1,42\ \text{interaction})} = 5.3$, $p = 0.026$; Tukey's tests, WT-naive vs WT-CFC: $p = 0.005$; KO-naive vs KO-CFC, $p = 0.99$; WT-naive vs KO-naive: $p = 0.31$; input-output gain: two-way ANOVA, $F_{(1,34\ \text{interaction})} = 8.8$, $p = 0.006$; Tukey's tests, WT-naive, $n = 9$, vs WT-CFC, $n = 10$: $p = 0.0001$, KO-naive, $n = 9$, vs KO-CFC, $n = 10$, $p = 0.89$; WT-naive vs KO-naive: $p = 0.99$; Figure 11*B*–*G*). SOM-INs from naive Som-Raptor-WT and Som-Raptor-KO mice showed similar spontaneous and evoked EPSCs (Mann–Whitney, spontaneous EPSC frequency: $p = 0.32$; minimally evoked EPSC potency: $p = 0.25$; Fig. 11*B*–*G*), indicating unchanged basal synaptic transmission. Furthermore, administration of the mGluR1 antagonist JNJ16259685 to Som-Raptor-WT mice 30 min before conditioning prevented the learning-induced potentiation (spontaneous EPSC frequency: vehicle, VEH: $n = 15$, JNJ: $n = 14$; Mann–Whitney, $p = 0.014$; amplitude: $t_{27} = 2.13$, $p = 0.0424$; minimally evoked EPSC potency: VEH: $n = 14$, JNJ: $n = 12$; $t_{24} = 5.31$, $p < 0.0001$; minimal stimulation intensity: $t_{24} = -4.32$, $p = 0.0002$; paired-pulse ratio: $t_{24} = -0.61$, $p = 0.55$; input-output gain: VEH: $n = 12$, JNJ: $n = 11$; Mann–Whitney, $p = 0.0092$; Fig. 11*H*). These results indicate that contextual fear learning induces mGluR1- and mTORC1-mediated persistent potentiation at SOM-INs excitatory synapses, suggesting that the effects of conditional genetic manipulations of mTORC1 on hippocampus-dependent memory and SOM-IN synaptic plasticity may be linked.

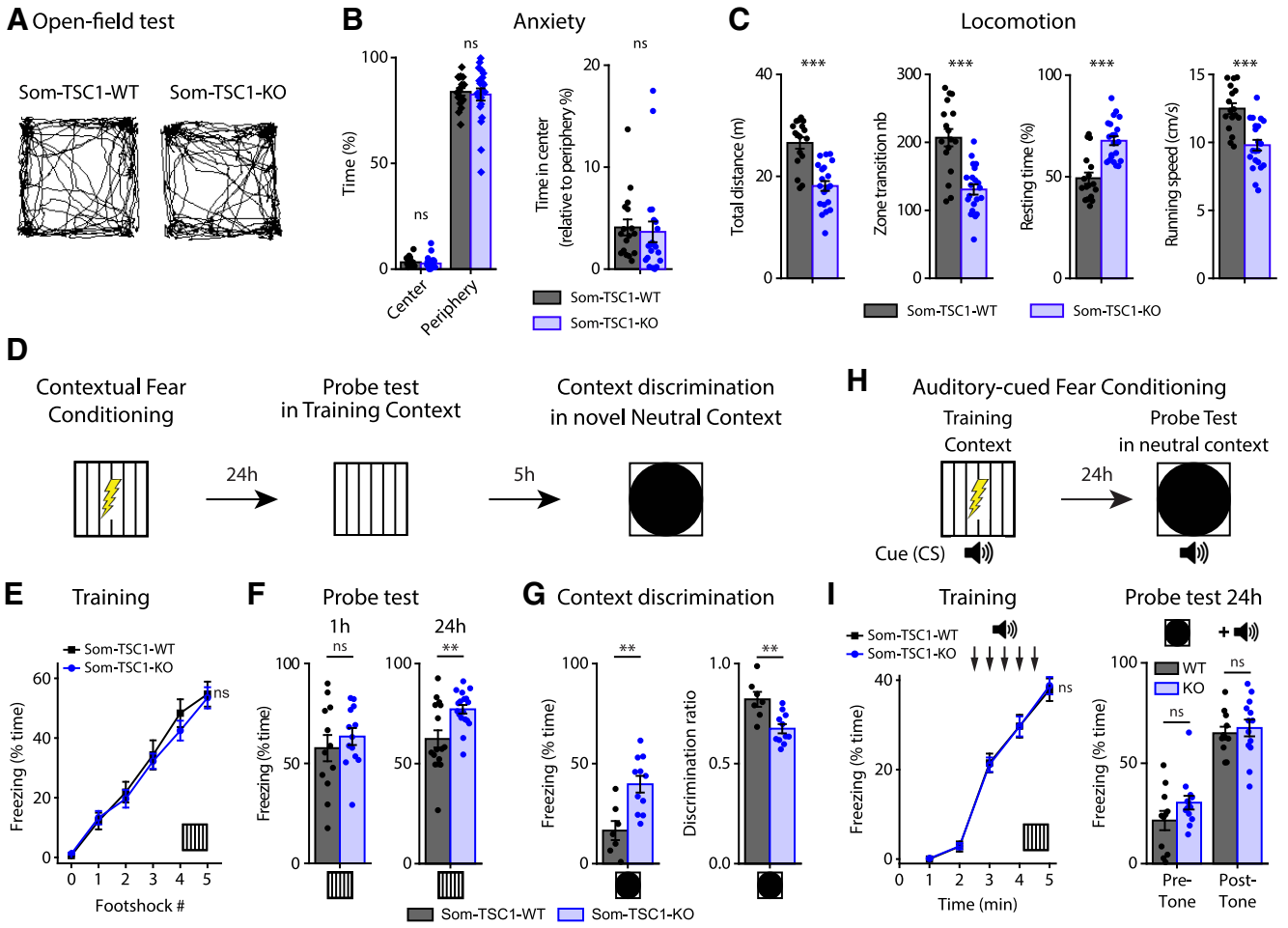

Figure 9. *Tsc1* deletion in SOM-INs increased long-term contextual fear memory but impaired context discrimination. ***A***, Representative paths traveled by Som-TSC1-WT (left) and Som-TSC1-KO (right) mice during 5 min free exploration in a square open-field. ***B***, Anxiety properties of Som-TSC1-WT and Som-TSC1-KO mice: percentage of time freezing in the center and in the periphery, and center/periphery ratio. ***C***, Locomotion properties of Som-TSC1-KO mice: total distance traveled, number of zone transitions, resting time and running speed. ***D***, Diagram of the contextual fear conditioning protocol. ***E***, Percentage of time freezing after each foot shock during the training session for Som-TSC1-WT and Som-TSC1-KO mice (0: before the first foot shock). ***F***, Percentage of time freezing during the probe tests at 1 h and at 24 h after conditioning. ***G***, Percentage of time freezing (left) and discrimination ratio (right) during the contextual discrimination test. ***H***, Diagram of the auditory-cued fear conditioning protocol. ***I***, Percentage of time freezing during the training session (left) and during the probe test 24 h after (right) for Som-TSC1-WT and Som-TSC1-KO mice. $^{**}p < 0.01$; $^{***}p < 0.001$; ns, not significant.

mTORC1-mediated late-LTP induction protocol in SOM-INs regulates SC-LTP in pyramidal cells

CA1 area is the output of the hippocampus and LTP at CA3-CA1 pyramidal cell synapses is considered a crucial phenomenon induced by learning and supporting memory (Whitlock et al., 2006; Choi et al., 2018). O-LM cells are a major subtype of dendrite-projecting SOM-INs (Pelkey et al., 2017) that provide differential regulation of SC and temporoammonic pathways onto CA1 pyramidal cells (Leão et al., 2012): they inhibit distal dendrites and downregulate LTP in the temporo-ammonic pathway; whereas they contact inhibitory interneurons in stratum radiatum and upregulate LTP at SC inputs (SC-LTP) by disinhibition (Leão et al., 2012; Vasuta et al., 2015; Hurtado-Zavala et al., 2017; Artinian and Lacaille, 2018). Consequently, induction of mGluR1a-mediated early-LTP at excitatory synapses onto SOM-INs upregulates SC-LTP of pyramidal cells, indicating that plasticity at SOM-INs input synapses regulates metaplasticity of the CA1 network (Vasuta et al., 2015). Therefore, we next examined whether mTORC1-mediated plasticity at SOM-IN input synapses controlled in a longer-lasting manner their output and regulated metaplasticity of the SC CA1 network. First, we established that late-LTP was elicited at SOM-INs synapses using electrical stimulation in acute slices (Fig. 12*A*). Repeated TBS stimulation at the oriens/alveus border in slices of Som-Raptor-WT mice induced, at 2 h postinduction, increases in EPSC amplitude (control: $n = 12$; TBS: $n = 12$; Mann–Whitney tests, $p = 0.004$) and potency ($p = 0.023$), and decreases in paired-pulse ratio ($p = 0.026$), relative to unstimulated slices (Fig. 12*B*,*C*). In contrast, SOM-INs from Som-Raptor-KO mice failed to show potentiation of EPSCs (control: $n = 11$; TBS: $n = 11$; Mann–Whitney, amplitude: $p = 0.74$; potency: $p = 0.65$; paired-pulse ratio: $p = 0.6$; Fig. 12*B*,*C*), indicating that late-LTP elicited by repeated TBS was mediated by mTORC1.

Having established a TBS protocol inducing mTORC1-mediated late-LTP in SOM-INs, we investigated its ability to control their output and upregulate SC-LTP of pyramidal cells in a persistent manner. We applied the repeated TBS induction protocol at the oriens/alveus border and 2 h later applied weak high-frequency stimulation (wHFS) in the stratum radiatum to induce SC-LTP in pyramidal cells (Fig. 12*D*). SC-LTP magnitude was increased in slices of Som-Raptor-WT that received 2 h previously the SOM-INs late-LTP induction protocol, relative to previously unstimulated slices (control: $n = 13$; TBS: $n = 15$; Mann–Whitney, $p = 0.03$; Fig. 12*G*,*I*). The upregulation of

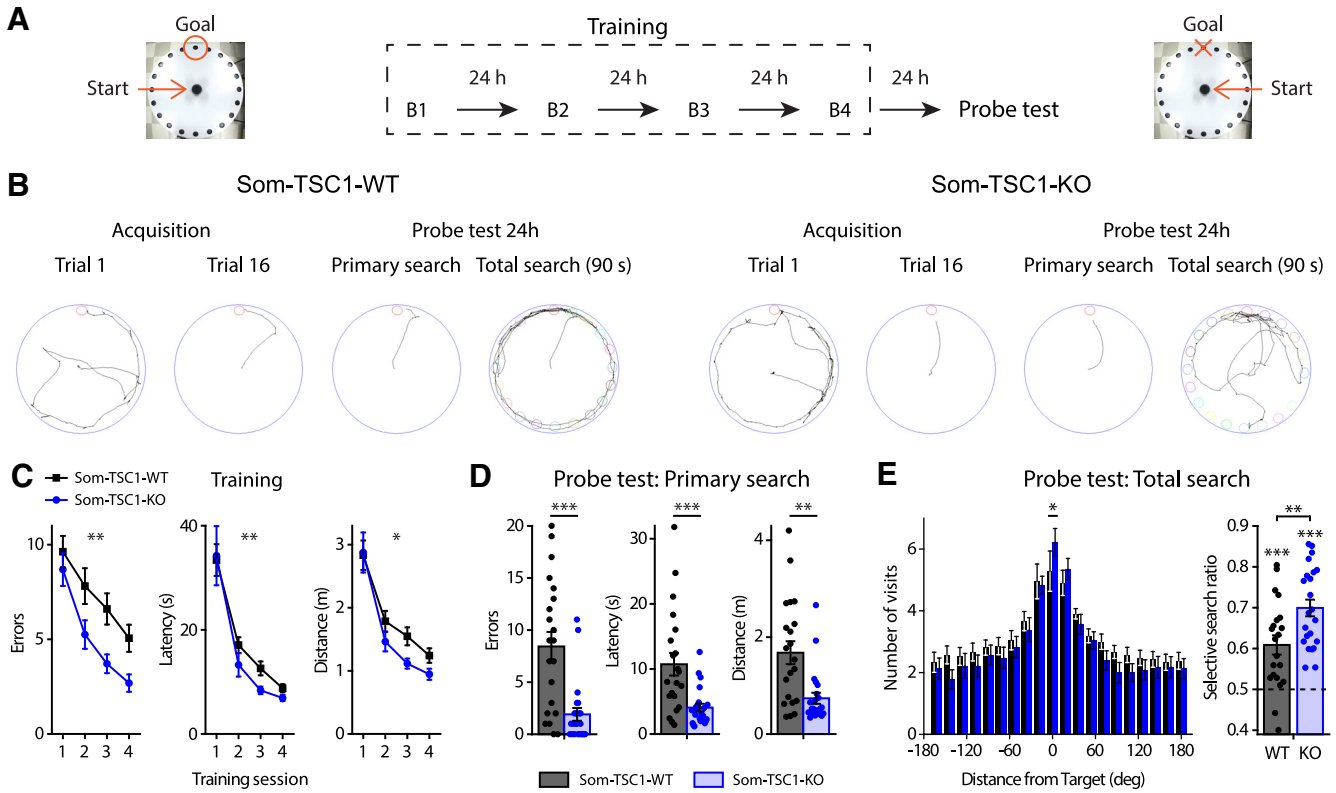

Figure 10. Som-TSC1-KO mice show enhanced spatial learning and long-term reference memory. ***A***, Diagram of the spatial learning protocol in the Barnes maze. ***B***, Left to right, Representative paths traveled by Som-TSC1-WT (left) and Som-TSC1-KO (right) mice during the first and last (16th) acquisition trials, as well as during the primary search and total search of the probe test. ***C***, Learning curves for Som-TSC1-WT and Som-TSC1-KO mice during the training session. ***D***, Memory performance during the primary search of the probe test. ***E***, Number of visits to all escape holes (left) and selective search ratio (right) during the total search of the probe test. $*p < 0.05$; $**p < 0.01$; $***p < 0.001$.

SC-LTP by repeated TBS was prevented in slices from Som-Raptor-KO mice (control: $n = 9$; TBS: $n = 13$; KO: Mann–Whitney, $p = 0.89$; WT vs KO: $t_{26} = 2.3$, $p = 0.029$; Fig. 12*H*,*I*), indicating that the upregulation of SC pathway plasticity required mTORC1-signaling, and thus likely mTORC1-mediated late-LTP, in SOM-INs. The block of SC-LTP regulation was not due to alterations in SC basal synaptic properties since input-output function (WT: $n = 9$; KO: $n = 10$; repeated two-way ANOVA, $F_{(8,135\ \text{interaction})} = 0.2$, $p = 0.7$; Fig. 12*E*) and paired-pulse facilitation (two-way ANOVA, $F_{(3,76)} = 0.39$, $p = 0.76$; Fig. 12*F*) were similar in Som-Raptor-KO and Som-Raptor-WT mice. These results show that repeated episodes of TBS induces long-lasting mTORC1-mediated plasticity at SOM-INs synapses that may result in long-lasting regulation of their output and CA1 network metaplasticity.

Together, our findings suggest that learning induces SOM-IN mTORC1 activity, resulting in persistent LTP at SOM-IN excitatory input synapses, and that this SOM-IN plasticity may in turn regulate CA1 SC synaptic plasticity. These SOM-IN mTORC1 cellular and circuit mechanisms could contribute to mTORC1 inhibitory circuit changes in contextual and spatial memory.

Discussion

We used cell-type specific transgenic mouse approaches to reveal several novel insights about mTORC1 activity in SOM-INs for hippocampal function. At the behavioral level, we uncovered that loss of mTORC1 function in SOM-INs impaired contextual fear and spatial long-term memories, but spared sensory-motor gating, hippocampus-dependent short-term contextual memory and hippocampus-independent long-term auditory-cued fear memory. In contrast, upregulation of mTORC1 activity in SOM-INs by cell-specific conditional knock-down of *Tsc1* augmented spatial and contextual fear memories, and impaired discrimination. At the cellular level, bidirectional regulation of mTORC1 activity in SOM-INs differentially regulated mGluR1-mediated late-LTP at SOM-IN excitatory inputs. Moreover, contextual fear learning persistently increased afferent excitatory synaptic strength in SOM-INs via mGluR1 and mTORC1. At the network level, the SOM-IN late-LTP induction protocol upregulated metaplasticity of the SC pathway in pyramidal cells, in mTORC1-dependent manner. Our findings uncover a role of SOM-IN mTORC1 in learning-induced plasticity of their synapses and in hippocampal long-term memory consolidation.

Raptor is an essential component of mTORC1 which plays a central role in cell growth (Saxton and Sabatini, 2017) in addition to regulation of protein synthesis during synaptic plasticity in mature neurons (Costa-Mattioli et al., 2009). *Rptor* deletion and *Tsc1* knock-down were not restricted in the hippocampus but occurred in all SOM-expressing cells and could possibly affect hippocampus-independent functions at the behavioral level. However, the intact anxiety, the moderate change in locomotion and the absence of freezing difference between WT and KO mice during CFC and short-term contextual fear memory indicate that hippocampus-independent functions such as sensorimotor gating and attention were spared in both conditional KO mice lines. Fear learning-induced synaptic potentiation in SOM-INs in the amygdala gates auditory-cued fear expression (Li et al., 2013; Penzo et al., 2015). We cannot rule out that genetic mTORC1 manipulations did affect SOM-INs physiology in the amygdala.

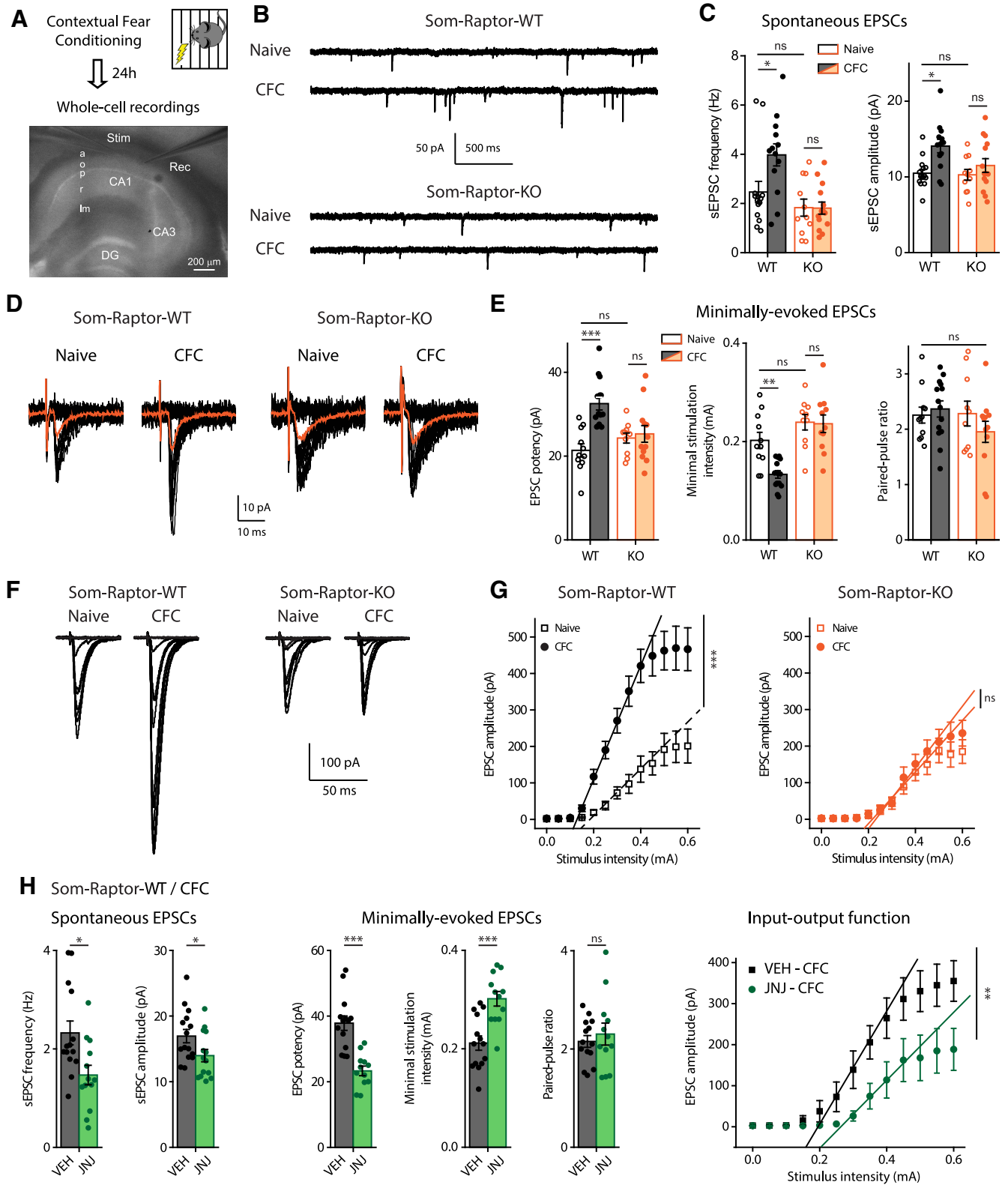

Figure 11. Contextual fear learning induces mGluR1- and mTORC1-mediated persistent LTP at excitatory synapses onto SOM-INs. ***A***, Diagram of the experimental protocol in acute slices. a, Alveus; o, oriens; p, pyramidale; r, radiatum; lm, lacunosum-moleculare; stim, stimulation pipette; rec, recording pipette. ***B***, Representative traces of spontaneous synaptic activity in SOM-INs from naive and trained Som-Raptor-WT and Som-Raptor-KO mice. ***C***, Spontaneous EPSC frequency and amplitude. ***D***, Representative traces of EPSCs evoked by minimal stimulation in the different conditions. ***E***, Minimally evoked EPSC potency, paired-pulse ratio and minimal stimulation intensity. ***F***, Representative traces of evoked input-output function in SOM-INs in the different conditions. ***G***, Input-output gain of SOM-INs as the slope of individual linear regressions. ***H***, Synaptic properties of SOM-INs from CFC-trained Som-Raptor-WT mice treated with mGluR1 antagonist JNJ16259685 relative to vehicle (VEH). $*p < 0.05$; $**p < 0.01$; $***p < 0.001$; ns, not significant.

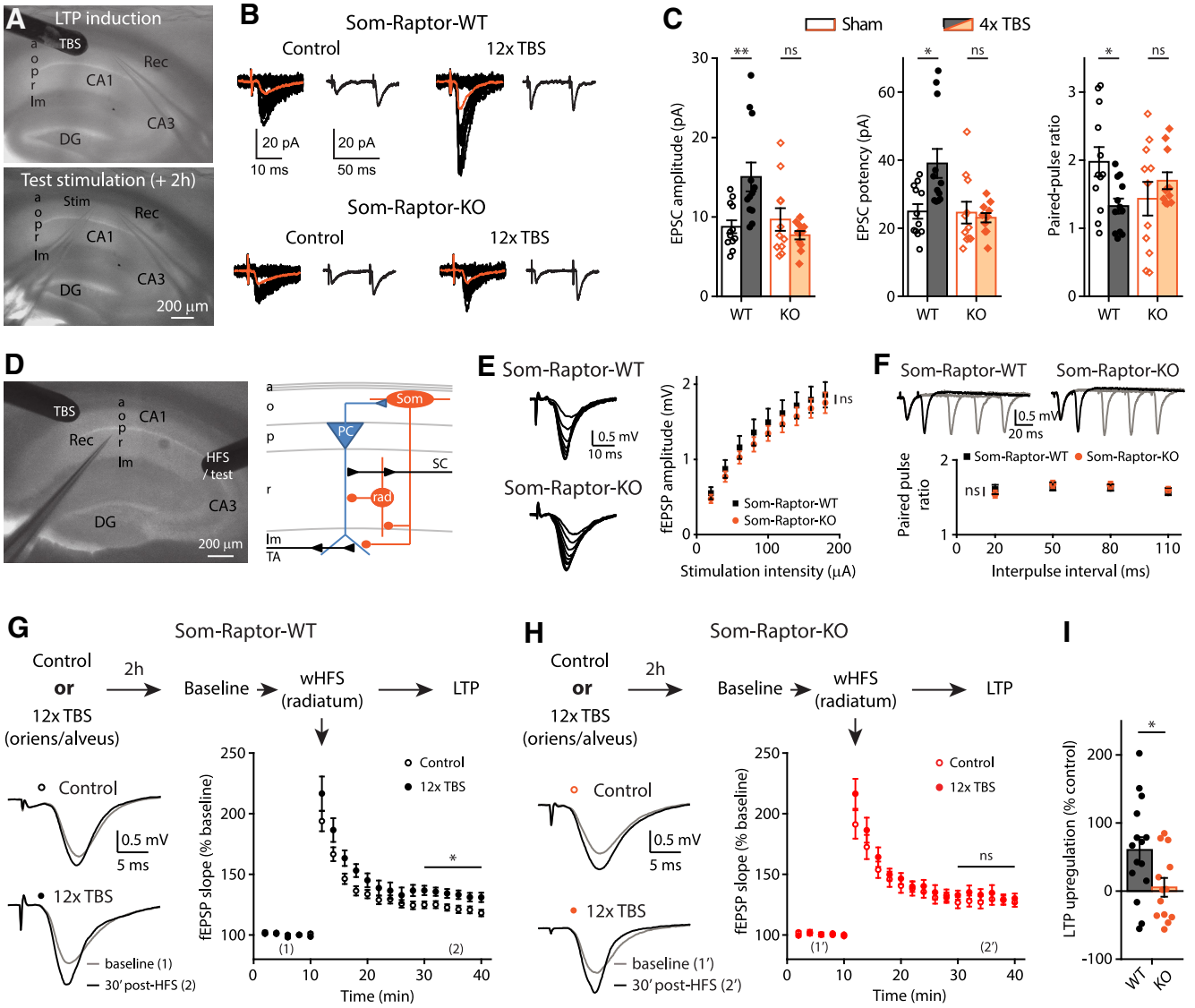

Figure 12. mTORC1-mediated late-LTP induction protocol in SOM-INs upregulates SC-LTP in principal cells. ***A***, Recording configuration for late-LTP induction and whole-cell recording 2 h later. ***B***, Representative traces of EPSCs evoked by minimal stimulation in control condition and after repeated TBS stimulation, in Som-Raptor-WT and Som-Raptor-KO mice. Traces are superimposed 20 consecutive events (EPSCs + failures, black), average EPSC (including failures, orange) and average of EPSC pairs (20 events) evoked by paired-pulse stimulation. ***C***, EPSC amplitude, potency (excluding failures) and paired-pulse ratio. ***D***, Recording configuration and simplified diagram of underlying CA1 network. SC: Schaffer collaterals, TA: temporo-ammonic pathway, PC: pyramidal cell, Som: SOM-INs, rad: radiatum interneuron. ***E***, Representative traces and amplitude of field EPSPs in response to incremental SC stimulation in Som-Raptor-WT and Som-Raptor-KO mice. ***F***, Representative traces and ratio of field EPSPs amplitude in response to SC paired-pulse stimulations. ***G***, Top: Description of the stimulation and induction protocol. Left: representative traces of field EPSPs in response to SC stimulation 10 min before (1) and 30 min after weak HFS (wHFS, 100 Hz, 750 ms) stimulation (2) to induce SC-LTP, in control condition and 2 h after the SOM-INs late-LTP induction protocol (repeated TBS stimulation) in Som-Raptor-WT mice. Right: Graph of LTP of field EPSP slope induced by wHFS. ***H***, Same as ***G*** in Som-Raptor-KO mice. ***I***, SC-LTP upregulation 2 h after SOM-INs late-LTP induction protocol, normalized to the averaged control SC-LTP. $*p < 0.05$; $**p < 0.01$; ns, not significant.

However in the present study, conditional deletion of *Rptor* and *Tsc1* knock-down in SOM-INs did not affect dorsal hippocampus-independent long-term auditory-cued fear memory. This indicates that learning-induced LTP in amygdala SOM-INs crucial for cued fear memory may not require mTORC1 mechanisms. Therefore, it would be interesting in future studies to examine mTORC1 function in amygdala SOM-INs to determine whether learning-related SOM-INs synaptic plasticity mechanisms are heterogeneous, with mTORC1 mechanisms specifically prominent in hippocampal SOM-INs synaptic plasticity.

Translational control by mTORC1 in synaptic plasticity and memory consolidation is well characterized in CA1 pyramidal cells (Costa-Mattioli et al., 2009). Our findings suggest that some aspects of mTORC1 function in synaptic plasticity are cell type-specific. We show that activation of mGluR1 in SOM-INs results in mTORC1-mediated late-LTP of excitatory synapses (Ran et al., 2009). However, activation of group I mGluRs in pyramidal cells was shown to induce mTORC1-mediated long-term depression of excitatory synapses (Banko et al., 2006). More recently, mTORC2 but not mTORC1 was associated with group I mGluR-mediated long-term depression (LTD) of CA1 pyramidal cells and novel object recognition (Zhu et al., 2018). Therefore, mGluR-mediated mTORC1, and perhaps even mTORC2, translational control likely regulates different mRNAs to achieve depression versus potentiation of synapses in pyramidal cells and SOM-INs, respectively. In addition, in other hippocampal interneurons which provides perisomatic inhibition of pyramidal cells, endocannabinoid-dependent long-term depression of their output synapses onto pyramidal cells requires presynaptic

mTORC1-mediated protein synthesis to downregulate GABA release (Younts et al., 2016). The identification of the downstream mechanisms and the specific mRNAs controlled by mTORC1 in different neurons classes will be important to clarify mTORC1 function in synaptic plasticity.

Cell type-specificity of mTORC1 function is consistent with findings that mTORC1 regulation of translation via one of its major effector, the translational repressor eukaryotic Initiation Factor 4E Binding Protein (eIF4E-BP), controls excitatory synaptic transmission differently in pyramidal cells and interneurons. In pyramidal cells, knock-out of eIF4E-BP results in enhanced basal excitatory synaptic transmission (Ran et al., 2013), as well as in a lower threshold for late-LTP induction and in impairment of late-LTP elicited by normal induction paradigms (Banko et al., 2005). In contrast, in hippocampal O-LM inhibitory interneurons, eIF4E-BP knock-out does not affect basal excitatory transmission, lowers the threshold for late-LTP induction and does not affect late-LTP elicited by normal induction paradigm (Ran et al., 2009). Our results in SOM-INs of Som-TSC1-KO mice are largely similar to those in eIF4E-BP knock-out. Conditional knock-down of *Tsc1* in SOM-INs increased mTORC1 activity as indicated by increase S6 phosphorylation in basal conditions. Moreover, the increased basal activity occluded mGluR1-induced mTORC1 activity in SOM-INs. Consistent with increased mTORC1 activity, the threshold for mGluR1-dependent late-LTP induction was lowered in SOM-INs of Som-TSC1-KO mice, with no change in basal excitatory transmission. Therefore, upregulated mTORC1 activity, in combination with ongoing synaptic activity, is not sufficient to increase synaptic strength and mGluR1 activation is also required. Interestingly, repeated mGluR1 activation failed to induce late-LTP in SOM-INs of Som-TSC1-KO mice, suggesting the presence of a mechanism of homeostatic control downstream of mTORC1, possibly via S6 kinase/4E-BP2/eIF4E pathways, to prevent excessive or unselective translation of mRNAs (Banko et al., 2005).

We demonstrated that Som-TSC1-KO mice manifested increased contextual fear and spatial memories as well as altered context discrimination, suggesting that upregulating mTORC1 activity in SOM-INs is sufficient to increase hippocampal memory consolidation. These effects of *Tsc1* knock-down are converse to those of *Rptor* deletion and suggest that the level of mTORC1 activity in SOM-INs determines the level of persistent synaptic plasticity in SOM-INs and memory consolidation. Since we found that rapamycin treatment reverses the electrophysiological abnormalities in Som-TSC1-KO, it would be interesting to examine in future studies if it could reverse also the behavioral abnormalities. Tuberous Sclerosis is a genetic disease due to mutation in TSC genes resulting in excessive mTORC1 activity and severe neurologic and psychiatric manifestations (Costa-Mattioli and Monteggia, 2013). Our findings in Som-TSC1-KO mice raise the interesting possibility that dysregulated mTORC1 activity and synaptic plasticity in SOM-INs contribute to cognitive impairments in tuberous sclerosis.

O-LM interneurons represent a major group of SOM-INs in CA1 hippocampus. They inhibit the distal temporo-ammonic inputs of pyramidal cells in stratum lacunosum-moleculare (Lovett-Barron et al., 2014; Pelkey et al., 2017), and send axonal projections in stratum radiatum to inhibit interneurons that, in turn, inhibit SC inputs of pyramidal cells (Leão et al., 2012). O-LM interneurons differentially control plasticity of the two inputs to pyramidal cells: they inhibit and restrict LTP of temporo-ammonic synapses; and they disinhibit and promote LTP of SC synapses (Leão et al., 2012; Vasuta et al., 2015; Hurtado-Zavala et al., 2017; Artinian and Lacaille, 2018). Hebbian mGluR1a-mediated LTP at excitatory input

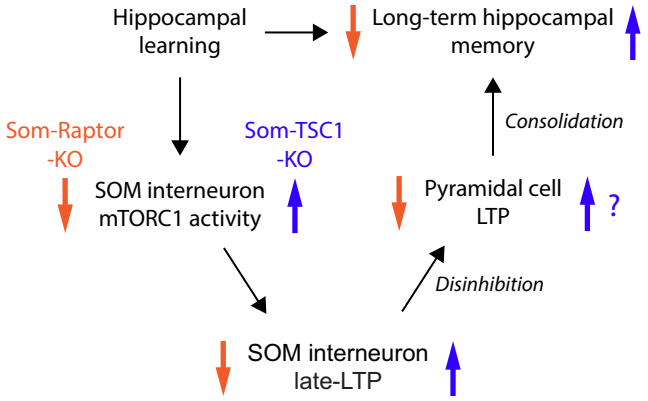

Figure 13. Model for regulation of hippocampal memory by mTORC1-mediated late-LTP in CA1 SOM interneurons. Hippocampal learning engages CA1 pyramidal cell firing that increases mGluR1-mediated mTORC1 activity in SOM-INs and induces Hebbian late-LTP at SOM-INs excitatory input synapses. Late-LTP in SOM-INs is then converted into increased output firing that upregulates LTP at SC synapses onto local pyramidal cells by disinhibition. Facilitated LTP in the CA1 principal pathway supports memory consolidation and promotes long-term hippocampal memory for future recall.

synapses onto O-LM interneurons is translated into increased synaptically driven action potential firing (Croce et al., 2010), providing a synaptic basis for increased inhibition of their downstream targets. Furthermore, induction of Hebbian mGluR1a-mediated LTP in SOM-INs upregulates for a period of minutes LTP in the SC pathway of pyramidal cells (Vasuta et al., 2015). Here we found that mTORC1-mediated late-LTP in SOM-INs upregulated for a period of hours LTP in the SC pathway. Interneurons expressing SOM in the CA1 hippocampus include not only O-LM cells but also bistratified cells and projection cells (Pelkey et al., 2017). In the present study, 90% of the biocytin labeled cells in our recordings were O-LM cells, clearly indicating a role of this interneuron subtype in SOM-IN mTORC1 actions in CA1. The development of new biological markers selective of other SOM interneuron subtypes will be necessary to assess their specific functional contributions.

We identified different physiological conditions in which mTORC1 activity is necessary for persistent enhancement of SOM-INs excitatory synapses: activation of mGluR1 in cultured (Ran et al., 2009, 2012) and acute slices, stimulation of afferent fibers in acute slices, and contextual fear learning. Our results suggest that the persistent potentiation of excitatory synapses onto SOM-INs elicited in these conditions share some common mechanisms. Contextual fear conditioning may engage activity of CA1 pyramidal cell excitatory synapses and activation of local SOM-INs to induce Hebbian mGluR1-mediated late-LTP at these synapses (Ran et al., 2009, 2012). Therefore, our results are consistent with a model (Fig. 13) that hippocampal learning: (1) induces persistent mGluR1 and mTORC1-mediated late-LTP at CA1 SOM-INs synapses due to coincident activation of presynaptic local pyramidal cells and postsynaptic SOM-INs, (2) resulting in a long-lasting disinhibition of SC inputs to pyramidal cells due to increased inhibition of intercalated inhibitory interneurons, effectively leading to an upregulation of CA1 network metaplasticity by enhancing LTP at pyramidal cell SC synapses, and (3) causing improved consolidation of accurate hippocampal memory. In association with long-term depression of inhibition from cholecystokinin (CCK)-positive interneurons in stratum radiatum (Basu et al., 2013), and with the action of long-range inhibitory projections from entorhinal cortex (Basu et al., 2016), mTORC1-mediated LTP in SOM-INs may be a complementary mechanism for disinhibition of SC inputs in pyramidal

cells (Artinian and Lacaille, 2018). Indeed during spatial navigation, it was recently reported that, as the animal crosses a place field, CA1 place cells decrease their synaptic coupling with parvalbumin-expressing interneurons and increase it with SOM-INs, causing a switch of pyramidal cell inhibition from perisomatic/proximal dendritic to distal dendritic compartments, and allowing CA3 excitatory inputs to gain control over entorhinal excitatory inputs in driving pyramidal cell firing in a short-term fashion (Fernandez-Ruiz et al., 2017). Therefore, a crucial feature of mTORC1-mediated SOM-INs plasticity in spatial/contextual information encoding by CA1 pyramidal cells may be to promote internal representations by the hippocampal CA3 pathway while dampening external representations via the extrahippocampal entorhinal inputs at longer time scales.

References

Abel T, Nguyen PV, Barad M, Deuel TA, Kandel ER, Bourtchouladze R (1997) Genetic demonstration of a role for PKA in the late phase of LTP and in hippocampus-based long-term memory. Cell 88:615–626.

Artinian J, Lacaille JC (2018) Disinhibition in learning and memory circuits: new vistas for somatostatin interneurons and long-term synaptic plasticity. Brain Res Bull 141:20–26.

Banko JL, Poulin F, Hou L, DeMaria CT, Sonenberg N, Klann E (2005) The translation repressor 4E-BP2 is critical for eIF4F complex formation, synaptic plasticity, and memory in the hippocampus. J Neurosci 25:9581–9590.

Banko JL, Hou L, Poulin F, Sonenberg N, Klann E (2006) Regulation of eukaryotic initiation factor 4E by converging signaling pathways during metabotropic glutamate receptor-dependent long-term depression. J Neurosci 26:2167–2173.

Barnes CA (1979) Memory deficits associated with senescence: a neurophysiological and behavioral study in the rat. J Comp Physiol Psychol 93:74–104.

Basu J, Srinivas KV, Cheung SK, Taniguchi H, Huang ZJ, Siegelbaum SA (2013) A cortico-hippocampal learning rule shapes inhibitory microcircuit activity to enhance hippocampal information flow. Neuron 79:1208–1221.

Basu J, Zaremba JD, Cheung SK, Hitti FL, Zemelman BV, Losonczy A, Siegelbaum SA (2016) Gating of hippocampal activity, plasticity, and memory by entorhinal cortex long-range inhibition. Science 351:aaa5694.

Choi JH, Sim SE, Kim JI, Choi DI, Oh J, Ye S, Lee J, Kim T, Ko HG, Lim CS, Kaang BK (2018) Interregional synaptic maps among engram cells underlie memory formation. Science 360:430–435.

Costa-Mattioli M, Monteggia LM (2013) mTOR complexes in neurodevelopmental and neuropsychiatric disorders. Nat Neurosci 16:1537–1543.

Costa-Mattioli M, Sossin WS, Klann E, Sonenberg N (2009) Translational control of long-lasting synaptic plasticity and memory. Neuron 61:10–26.

Croce A, Pelletier JG, Tartas M, Lacaille JC (2010) Afferent-specific properties of interneuron synapses underlie selective long-term regulation of feedback inhibitory circuits in CA1 hippocampus. J Physiol 588:2091–2107.

Fernandez-Ruiz A, Oliva A, Nagy GA, Maurer AP, Berényi A, Buzsáki G (2017) Entorhinal-CA3 dual-input control of spike timing in the hippocampus by theta-gamma coupling. Neuron 93:1213–1226.e5.

Fox GB, Fan L, LeVasseur RA, Faden AI (1998) Effect of traumatic brain injury on mouse spatial and nonspatial learning in the Barnes circular maze. J Neurotrauma 15:1037–1046.

Hurtado-Zavala JI, Ramachandran B, Ahmed S, Halder R, Bolleyer C, Awasthi A, Stahlberg MA, Wagener RJ, Anderson K, Drenan RM, Lester HA, Miwa JM, Staiger JF, Fischer A, Dean C (2017) TRPV1 regulates excitatory innervation of OLM neurons in the hippocampus. Nat Commun 8:15878.

Kandel ER, Dudai Y, Mayford MR (2014) The molecular and systems biology of memory. Cell 157:163–186.

Kullmann DM, Moreau AW, Bakiri Y, Nicholson E (2012) Plasticity of inhibition. Neuron 75:951–962.

Leão RN, Mikulovic S, Leão KE, Munguba H, Gezelius H, Enjin A, Patra K, Eriksson A, Loew LM, Tort AB, Kullander K (2012) OLM interneurons differentially modulate CA3 and entorhinal inputs to hippocampal CA1 neurons. Nat Neurosci 15:1524–1530.

Li H, Penzo MA, Taniguchi H, Kopec CD, Huang ZJ, Li B (2013) Experience-dependent modification of a central amygdala fear circuit. Nat Neurosci 16:332–339.

Lovett-Barron M, Turi GF, Kaifosh P, Lee PH, Bolze F, Sun XH, Nicoud JF, Zemelman BV, Sternson SM, Losonczy A (2012) Regulation of neuronal input transformations by tunable dendritic inhibition. Nat Neurosci 15:423–430, S421–S423.

Lovett-Barron M, Kaifosh P, Kheirbek MA, Danielson N, Zaremba JD, Reardon TR, Turi GF, Hen R, Zemelman BV, Losonczy A (2014) Dendritic inhibition in the hippocampus supports fear learning. Science 343:857–863.

Nicoll RA (2017) A brief history of long-term potentiation. Neuron 93:281–290.

Pelkey KA, Chittajallu R, Craig MT, Tricoire L, Wester JC, McBain CJ (2017) Hippocampal GABAergic inhibitory interneurons. Physiol Rev 97:1619–1747.

Pelletier JG, Lacaille JC (2008) Long-term synaptic plasticity in hippocampal feedback inhibitory networks. Prog Brain Res 169:241–250.

Penzo MA, Robert V, Tucciarone J, De Bundel D, Wang M, Van Aelst L, Darvas M, Parada LF, Palmiter RD, He M, Huang ZJ, Li B (2015) The paraventricular thalamus controls a central amygdala fear circuit. Nature 519:455–459.

Perez Y, Morin F, Lacaille JC (2001) A hebbian form of long-term potentiation dependent on mGluR1a in hippocampal inhibitory interneurons. Proc Natl Acad Sci U S A 98:9401–9406.

Polepalli JS, Wu H, Goswami D, Halpern CH, Südhof TC, Malenka RC (2017) Modulation of excitation on parvalbumin interneurons by neuroligin-3 regulates the hippocampal network. Nat Neurosci 20:219–229.

Ran I, Laplante I, Bourgeois C, Pépin J, Lacaille P, Costa-Mattioli M, Pelletier J, Sonenberg N, Lacaille JC (2009) Persistent transcription- and translation-dependent long-term potentiation induced by mGluR1 in hippocampal interneurons. J Neurosci 29:5605–5615.

Ran I, Laplante I, Lacaille JC (2012) CREB-dependent transcriptional control and quantal changes in persistent long-term potentiation in hippocampal interneurons. J Neurosci 32:6335–6350.

Ran I, Gkogkas CG, Vasuta C, Tartas M, Khoutorsky A, Laplante I, Parsyan A, Nevarko T, Sonenberg N, Lacaille JC (2013) Selective regulation of GluA subunit synthesis and AMPA receptor-mediated synaptic function and plasticity by the translation repressor 4E-BP2 in hippocampal pyramidal cells. J Neurosci 33:1872–1886.

Royer S, Zemelman BV, Losonczy A, Kim J, Chance F, Magee JC, Buzsáki G (2012) Control of timing, rate and bursts of hippocampal place cells by dendritic and somatic inhibition. Nat Neurosci 15:769–775.

Ruediger S, Vittori C, Bednarek E, Genoud C, Strata P, Sacchetti B, Caroni P (2011) Learning-related feedforward inhibitory connectivity growth required for memory precision. Nature 473:514–518.

Saxton RA, Sabatini DM (2017) mTOR signaling in growth, metabolism, and disease. Cell 169:361–371.

Schmid LC, Mittag M, Poll S, Steffen J, Wagner J, Geis HR, Schwarz I, Schmidt B, Schwarz MK, Remy S, Fuhrmann M (2016) Dysfunction of somatostatin-positive interneurons associated with memory deficits in an Alzheimer's disease model. Neuron 92:114–125.

Sunyer B, Patil S, Höger H, Lubec G (2007) Barnes maze, a useful task to assess spatial reference memory in the mice. Protocol Exchange. Advance online publication. Retrieved October 4, 2007. doi: 10.1038/nprot.2007.390.

Tricoire L, Pelkey KA, Erkkila BE, Jeffries BW, Yuan X, McBain CJ (2011) A blueprint for the spatiotemporal origins of mouse hippocampal interneuron diversity. J Neurosci 31:10948–10970.

Vasuta C, Artinian J, Laplante I, Hébert-Seropian S, Elayoubi K, Lacaille JC (2015) Metaplastic regulation of CA1 Schaffer collateral pathway plasticity by Hebbian MGluR1a-mediated plasticity at excitatory synapses onto somatostatin-expressing interneurons(1,2,3). eNeuro 2:ENEURO.0051-15.2015.

Whitlock JR, Heynen AJ, Shuler MG, Bear MF (2006) Learning induces long-term potentiation in the hippocampus. Science 313:1093–1097.

Wiltgen BJ, Silva AJ (2007) Memory for context becomes less specific with time. Learn Mem 14:313–317.

Younts TJ, Monday HR, Dudok B, Klein ME, Jordan BA, Katona I, Castillo PE (2016) Presynaptic protein synthesis is required for long-term plasticity of GABA release. Neuron 92:479–492.

Zhu PJ, Chen CJ, Mays J, Stoica L, Costa-Mattioli M (2018) mTORC2, but not mTORC1, is required for hippocampal mGluR-LTD and associated behaviors. Nat Neurosci 21:799–802.